RECEIVED BY TIO FEB 5 1980

LBL-9990

Lawrence Berkeley Laboratory

UNIVERSITY OF CALIFORNIA

Materials & Molecular Research Division

A MODEL OF THE RECRYSTALLIZATION MECHANISM OF AMORPHOUS SILICON LAYERS CREATED BY ION IMPLANTATION

Robert M. Drosd
(Ph.D. thesis)

MASTER

November 1979

Prepared for the U.S. Department of Energy under Contract W-7405-ENG-48

DISTRIBUTION OF THIS DOCUMENT IS UNLIMITED

DISCLAIMER

TABLE OF CONTENTS

ABSTRACT

1. Introduction 1

1.1 Amorphous Layer Formation. 1

1.2 Annealing Behavior of Conventional Wafers. 3

1.3 A New Model for Amorphous Layer Regrowth 4

1.4 A New Experimental Technique 5

2. Experimental Procedure 7

2.1 Ion Implantation Procedure and Starting Materials. 7

2.2 Annealing Procedure. 8

2.3 Specimen Preparation 8

2.4 Specimen Geometry. 8

3. Results, Conventional Specimens. 10

3.1 Implantation at Liquid Nitrogen Temperature. 10

3.2 Room Temperature Implantation. 12

3.3 100°C Implants 12

3.4 The Depth of Lattice Defects in Annealed Wafers. . . . 13

4. Discussion 15

4.1 A Model for Amorphous Layer Regrowth 15

a Substrate Orientation Effects. 15

b Implantation Temperature Effects 19

4.2 The Defect Formation Mechanism During Amorphous Layer Regrowth. 21

a Dislocation Loops and Networks 21

b Microtwins 22

DISTRIBUTION OF THIS DOCUMENT IS UNLIMITED

4.3 Comparison of Experimental Results to Model Predictions 24

a Regrowth Rate 24

b Defect Microstructures. 24

4.4 Other Models for Amorphous Layer Regrowth 25

5. Introduction and Results, TFA Specimens. 27

5.1 Results of (001) TFA Specimens. 27

5.2 (111) TFA Samples 29

5.3 (110) TFA Samples 30

5.4 General Observation of TFA Specimens. 31

a Contamination Effects 31

b The Effect of Curvature on the Growth Rate. 32

c Oriented Crystallites in Advance of the α/C Interface 32

6. Discussion of Thin Foil Annealed Amorphous Layer Regrowth. 34

6.1 Complications in evaluating the TFA Experiment. . . . 34

a α/C Interface Rotation and Faceting 34

b The Effect of α/C Interface Curvature on the Regrowth Rate. 36

c The Effect of the Doping Profile. 37

6.2 Comparison of Data From Conventional and TFA Samples 38

a Numerical Data. 38

b Defect Microstructures. 40

7. Conclusions. 42

7.1 Summary of this Work. 42

7.2 Applications to Practical Problems. 42

7.3 Suggestions for Further Work. 43

Acknowledgements 48

References 49

Figure Captions. 53

A MODEL OF THE RECRYSTALLIZATION MECHANISM OF AMORPHOUS SILICON LAYERS CREATED BY ION IMPLANTATION

Robert M. Drosd

Materials and Molecular Research Division,
Lawrence Berkeley Laboratory,
University of California,
Berkeley, CA 94720

ABSTRACT

The recrystallization behavior during annealing of thin films of amorphous (α) silicon, in contact with a single crystal silicon substrate (referred to as C), has been studied in the transmission electron microscope (TEM). The amorphous film is created during high dose phosphorus ion implantation at 100 keV. It was found that the crystal substrate orientation and the implantation temperature have dramatic effects on the recrystallization rate, and the defect microstructure produced during annealing. Specifically, (100) wafers implanted at 77°K contain only a low density of dislocation loops, but when the same wafer is implanted at room temperature the dislocation density is increased drastically. (111) wafers, when implanted at 77°K show a high density of microtwins, but as the implantation temperature is increased a gradual increase in the density of dislocation loops is observed along with a reduction of the microtwins. At an implantation temperature of about 100°C both orientations give an identical defect microstructure when annealed, which is a dense tangle of dislocations.

An atomistic model has been developed to explain the results mentioned above. The atomic bond structure at the α/C interface is discussed as a function of the substrate orientation. From

considerations of this type it is seen that the critical number of atoms to form a stable nucleus for a new atomic layer on the crystalline surface is one for the (100) face but is three for (111). In addition, on the (111) surface two possible positions exist in which the new atomic layer may begin, one of which forms a twin boundary. According to this model, twinning should be expected only for a (111) substrate, which is the experimental observation.

The effect of implantation temperature on the annealed microstructure is a result of the roughness of the α/C interface. It is observed experimentally that the interface roughness increases with the implantation temperature. If the roughness is severe then the interface is no longer required to regrow in a direction normal to itself. It is for this reason that twinning is avoided for the (111) wafers implanted at high temperatures.

A new <u>in situ</u> TEM technique is introduced where layer regrowth was observed and the role that defects play during recrystallization was identified. Numerical data on the α layer regrowth rate were obtained in the TEM for the first time.

1. INTRODUCTION

This thesis is a study of the atomic mechanisms that are responsible for the recrystallization of thin films of amorphous (α) silicon in contact with a single crystal substrate during annealing. Thin films of amorphous materials may be formed by several techniques such as vapor deposition, sputtering, and ion implantation.[1,2] The latter will be used in this study since it allows for precise impurity control and avoids the possibility of an oxide or contamination layer at the crystalline amorphous (α/C) interface. In addition the recrystallization of α layers created by ion implantation is of practical importance to the semiconductor industry[3,4] where the current lack of control of the regrowth process results in poor epitaxial regrowth which degrades the electrical properties of recrystallized silicon wafers.

1.1 Amorphous Layer Formation

Although ion irradiation is only being used as a means to produce α silicon it is necessary to have a basic understanding of the implantation process to better evaluate the initial configuration of the α layer. The following section includes a discussion of the radiation damage process and some of its important parameters. Ion implantation of dopant atoms is generally conducted in the accelerating energy range from 20 to 200 thousand electron volts. The corresponding depth of penetration[5] of the ions into the silicon target will be on the order of a few hundred to a few thousand angstroms, depending on the accelerating voltage and the mass of the implanted

ion; lighter ions penetrating further. Upon entering the target lattice, the incident ions will at first suffer few atomic collisions due to their high velocity but will lose energy slowly by ionizing the host atoms. As the ion energy is reduced the probability of nuclear collisions increases. Hence, after traveling some distance without causing atomic displacement, they undergo a catastrophic loss in energy due to nuclear collisions with the target lattice atoms. This results in the formation of a large number of interstitial atoms and vacant lattice sites.[6] As a result the crystal is most heavily damaged at a depth near R_p where R_p is the average range of the incident ions.

If the implantation dose is greater than a critical level an amorphous layer is formed which is on the order of $2R_p$ in thickness.[7] The mechanism by which it is formed is not yet certain but two plausible theories exist. The first[8] proposes that near the end of each ion track a small amorphous zone is created. As the number of implanted ions increases the density of these zones reaches a point where they overlap and a continuous amorphous layer is created. The second theory[9] assumes that although the individual ions create a high density of point defects near the end of their path, the target remains crystalline. However, when a critical density of defects is reached, the lattice transforms to an amorphous structure as a phase transformation to a metastable state.

There are several variables that affect the ion dose required to form an amorphous layer. The ion species is critical[10] in that

heavy ions cause amorphitization more readily. Low implantation temperatures[11] also facilitate the disordering of the crystal during bombardment. The ion accelerating voltage[12] is not of major importance in determining the critical dose. Crystal orientation in general is also found not to affect the amorphitization process. If the incident ions are so aligned that they can travel along low index crystal directions, their range is increased substantially[13] and hence the density of damage at any particular depth decreases. For this reason channeled implants require higher doses to form amorphous layers. Each of the above mentioned parameters affecting amorphous layer formation will be discussed later in relation to the results of to the present investigation.

1.2 Annealing Behavior of Conventional Wafers

If an implanted silicon wafer is to serve as a solid state electronic device it must be annealed to return the displaced atoms including the implanted dopant atoms to subsitutional sites.[14] The conventional technique for annealing silicon wafers containing amorphous layers is in a furnace under an inert atmosphere. High power pulsed lasers[5] and electron beams have also come into use recently but will not be discussed here. An amorphous layer in silicon will recrystallize completely in a reasonably short time (1 hour) at about 500° to $550^{o}C$. Unfortunately it is found that only under very special implantation conditions will the regrown layer be low in defects.[16] In general a high density of dislocations, stacking faults, microtwins, and dislocation loops are found which

degrade the electrical properties. It has been shown[17-19] that there is a strong effect of the crystal substrate orientation on the types and densities of defects found after annealing. Good defect-free epitaxial regrowth has only been observed for (100) substrates implanted at low temperatures.

In addition it has been observed in the present work that the implantation temperature affects the a/C interface roughness which in turn affects the defect structures found after annealing. This is puzzling since the implantation temperatures of interest are all at least 500^{0}C lower than those of the subsequent annealing treatment. Ion species and dose effects exist as well.[20-23] Many of these observations mentioned above are not new but a model that explains how they arise is lacking.[24] It is the major goal of this study to shed some light on the atomic processes that are active during recrystallization and therefore to be able to explain the profound effects of implantation temperature and substrate orientation.

1.3 A New Model for Amorphous Layer Recrystallization

A model has been constructed that satisfactorily explains the major observations concerning the recrystallization of thin films of amorphous silicon during furnace annealing. Previous models have had some success[24] in explaining the experimental observations but, in general, they have only applied to a particular set of experimental conditions. The model presented here is broader in scope than those published to date.

The model is based on three fundamental ideas: Of first importance is the arrangement of near neighbors at various orientations of the surface of a crystal. The density of sites at which a single atom can become strongly attached to the crystal so as to be considered to be part of the crystal depends on the crystallographic orientation of the face.[25] It will be shown that this can explain the orientation dependence of the recrystallization rates of α layers in silicon.

The second concept involved is that the probability of nucleating stacking mistakes that lead to microtwinning also depends critically on the crystallographic orientation of the growing crystal face.[26] These two concepts are related in that formation of microtwins can in certain orientations increase the density of sites at which atoms can join the crystal.

The third basis for the model depends on the experimental observation that the implantation temperature effects the roughness of the α/C interface The consequences of this will be discussed in detail in a later section.

1.4 A New Experimental Technique

To gain a greater insight into the mechanisms of α layer recrystalization a new experimental technique has been developed for observing the motion of the α/C interface during annealing. The details of this technique will be given later but, briefly, this is an in situ transmission electron microscope study incorporating a unique specimen geometry that allows for the simultaneous measurement of the migration rate of the α/C interface along with observation of any

crystal defects that are formed and their affects on the recrystallization process. Previous studies using the transmission electron microscope[27] (TEM) have all been performed after annealing was complete and hence could only serve to identify the final configuration of defects. Rutherford backscattering (RBS) growth rate measurements[28] can be made during annealing but only the average position of the α/C interface may be measured; using this technique no understanding of the origin or role of defects is possible.

2. EXPERIMENTAL PROCEDURE

2.1 Ion Implantation Procedure and Starting Materials

N type (2-5 ohm-cm) silicon wafers were obtained from a commercial supplier (Monsanto). They were in the form of 3" discs of .017" thickness. Prior to implantation they were cleaned using the "Pirana"[29] etch followed by boiling TCE (Trichloroethylene) and a rinse in distilled water. The wafers were then attached to the ion implantation specimen holder using a heat conducting paste containing SnO manufactured by Dow Corning. This was to insure good thermal contact to the holder. It should be noted that this paste tends to form bubbles under the wafer when placed in the vacuum. Hence, the thermal contact is not as good as it might otherwise be. Silver conducting paint works well at room temperature but cannot be used for low temperature implants because it is not flexible enough to accomodate the difference in thermal expansion of the silicon wafer and metal specimen holder.

During implantation the accelerating voltage was kept at 100 kV, the ion current ranged from 1 to 3 $\mu A/cm^2$ giving an input power of 0.1 to 0.3 $watts/cm^2$. Calculations[30] show that, for radiation cooling only, the temperature of the wafer would rise by several hundred degrees centigrade due to the incident ion beam energy imput. It is for this reason that the heat conducting paste was used. It is more difficult to estimate the surface temperature when good thermal contact is established but the rise in temperature above ambient is expected to be small.

2.2 Annealing Procedure

Samples were annealed in a conventional tube furnace with a flowing nitrogen atmosphere. A thermocouple placed beside the specimen allowed the temperature to be controlled within two degrees of the desired temperature.

2.3 Specimen Preparation

After implantation the wafers were cut with an ultrasonic impact grinding tool into 3 mm discs for use as TEM specimens. In addition, a one mm diameter "dimple" was formed in the center of the specimen to a depth of .005" on the unimplanted side. For chemical thinning, the 3 mm discs were placed implanted side down on a thin piece of teflon sheet and covered in molten wax. Immediately after solidification, the dimpled area is scratched free of wax leaving only the "dimple" exposed. The teflon sheet and specimen was then immersed in an acid bath of 1 part solution A (2.5 g Iodine, 1100 ML CH_3OOH) and 2 parts solution B (1 part HF, 3 parts HNO_3), and a bright light was placed below the acid containing beaker. As the silicon reaches a thickness of about 1 micron at the center it transmits enough red light to be visible thus warning that perforation is imminent. As soon as a small hole appeared, the sample was rapidly placed in water and rinsed. The specimen was then removed from the wax and cleaned by placing it in boiling TCE for a short time.

2.4 Specimen Geometry

Two different types of specimens were used in this study. The first type, which will be called the conventional TEM specimen, was produced as described in the previous section after annealing. Since

the specimen is annealed prior to thinning the amorphous layer is recrystallized and may contain defects which will be exposed in the thin area of the wedged shape specimen as shown in Fig. 1a. The plane of the specimen and the original α/C interface are parallel. The vast majority of TEM investigations of ion implanted silicon to date have been made using the conventional specimen geometry.

A new type of TEM specimen, which will be referred to as the "Thin Foil Annealed" (TFA) specimen has been developed for use in studying the regrowth of amorphous layers. The specimen was cut and chemically thinned in exactly the same manner as the conventional specimen described above. However, the TFA specimen was thinned prior to annealing. This resulted in an exposed portion of the α layer that was not superimposed on the crystalline substrate as shown in Fig. 1b. Regrowth during annealing takes place by the motion of the α/C interface from the parent crystal. Initially the superimposed α material is consumed and then the interface gradually turns by 90° and moves toward the hole in the center of the specimen, see Fig. 2. It is at this stage that the α/C interface is seen to sweep across the field of view. As this occurs, the interface can be observed at different positions around the edge of the hole in the specimen, representing regrowth in all the crystalographic directions contained in the plane of the foil. (See Fig. 3). By annealing a single TFA specimen and taking sequential micrographs one may measure the regrowth rate of the α layer in several different growth directions. Further results and discussion of the TFA experiments will be deferred until Section 5.

3. RESULTS, CONVENTIONAL SPECIMENS

The conventional TEM specimen, as described in Section 2.4, is very important in that it shows the type of defects that are produced in ordinary ion implanted and annealed wafer. This type of specimen was made from wafers of (100), (110), and (111) orientation at implantation temperatures ranging from 77° to $400^{o}K$. The dose was also varied over a considerable range but was found to be of major importance only in the sense that below a critical dose, no a layer was formed. The critical dose for amorphitization is a function of implantation temperature and has been experimentally measured,[11] as shown in Fig. 4. Most of the results presented here were obtained for a dose of 10^{16} ions/cm^2 which is sufficient to form an amorphous layer up to about $100^{o}C$ implantation temperature. Above the critical value the dose was found to affect the density but not the type of defects found. The implantation temperature was found to have a strong effect on both the nature and density of defects, therefore the results will be divided according to the temperature at which the implantation was carried out. In the last part of the results section data concerning the depth of the defects in the wafer will be presented.

3.1 Liquid Nitrogen Implantation

Figure 5a,b,c shows a (111), (110), and (100) wafer implanted to a dose of $10^{16}P/cm^2$ and annealed at $800^{o}C$ for 1/2 hour. The (111) sample shows a high density of plate like microtwins while the other two orientations contain only dislocation loops. Some of the loops

are faulted while others have perfect burgers vectors. The nature of these loops was not determined in this study, but, has been shown to be interstitial by other investigators.[31] The microtwins in the (111) sample have been measured by other workers[32] and found to be on the order of a few hundred angstroms thick lying on the three inclined (111) planes. Some twins were also found in the plane of the wafer and were more blocky in shape. The α layer created during a 100 kV, 10^{16} phosphorus ions/cm^2 implantation at $77^{o}K$ was about 2000Å thick, hence the plate-like twins extend about this distance in one direction but were considerably longer in the direction parallel to the plane of the wafer. In Fig. 5 the electron diffraction pattern is shown from the (111) sample containing microtwins along with the (110) pattern obtained from the same specimen by tilting it 35°. Both serve to show the high density of twin spots and streaking which arrise from the plate-like shape of the twins.

The unannealed structure of a wafer implanted at $77^{o}K$ is shown in Fig. 6. All the wafer orientations studied were identical in the unannealed state. The α layer was homogeneous and appeared to be featureless. At a distance from the edge of the specimen the superimposed crystal substrate is encountered. In dark field, Fig. 6b, faint bright objects are visible in the region where the crystalline and α material overlapped. The most likely explanation for these bright spots is that they are strained regions of the crystal that penetrate into the α layer at the α/C interface as shown schematically in Fig. 6c. Amorphous silicon is somewhat less dense than the

crystalline material so there will be strain at the interface. The size and density of the bright spots seen in the dark field micrograph can be used as an indication of the interface roughness.

3.2 Room Temperature Implantation

When the implantation temperature was held at room temperature, rather than $77^{o}K$, the annealed microstructures were considerably different. In Fig. 7a the (111) sample still contains microtwins but some dislocations are seen as well. The other two orientations, shown in Fig. 7b & c, both have a greater density of dislocation loops, than the $77^{o}K$ implant, some of which have intersected one another. In Fig. 7d the unannealed structure is shown where the α and crystalline materials overlap. The size of the bright spots mentioned in the previous section has increased indicating a larger scale of roughness of the α/C interface.

3.3 $100^{o}C$ Implants

At an implantation temperature of $100^{o}C$, the defect type and density in the annealed wafers is identical for all three major orientations as shown in Fig. 8. Here a high density of dislocation loops, many of which have intersected one another, is seen. If annealing was carried out longer or at higher temperatures a well defined network of edge dislocations was formed as seen in Fig. 9.

The unannealed structure, Fig. 8d, shows very large bright spots indicating a still rougher α/C interface than at either lower implantation temperature. The α layer does not reach the implanted surface of the wafer in this case. Hence the material is buried beneath a thin crystalline layer and two α/C interfaces exist.

3.4 The Depth of Lattice Defects in Annealed Wafers

It has already been pointed out that the implantation temperature can affect the type of defects formed during annealing. In this section micrographs are presented that indicate the relative depths in the specimens at which these defects were found. Since a conventional TEM specimen is always wedge shaped (Fig. 1) the region of the sample near the edge of the hole represents the top surface. What was seen in the region far removed from the edge was a superposition of defects at all depths in the recrystallized α layer. With this understanding of specimen geometry, the relative depths of different layers of defects found in conventional specimens was determined. This information will be of importance later on in Section 4.1b where a model for implantation temperature effects is presented.

Figure 10a is a wedge shaped (111) conventional specimen that has been implanted at 77°K and then annealed at 800°C for 1/2 hour. The insets show higher magnification images of the thick and thin areas. Microtwins are seen at all depths of the specimen. Figure 10b is an identical sample except it has been implanted at room temperature. Here twins are still seen in the thin area but in the thick region, representing regions of greater depth in the specimen as well, a dislocation network is found in addition to the twins. Hence in the room temperature implanted (111) wafer, dislocations lie beneath the microtwins.

Figure 11a is a (100) sample that has been implanted at 77°K. Dislocation loops are seen but only in an area far removed from the

specimen edge. Therefore, these loops are fairly deep in the wafer, probably near the original α/C interface. Figure 11b shows an identical sample except it has been implanted at 100°C. Here a dislocati network is seen that extends very near to the specimen edge. This network must extend over a much wider range of depth then the loops in Fig. 11a.

4. DISCUSSION

4.1 A Model for Amorphous Layer Regrowth

In this section a model for the recrystallization mechanism of a silicon will be described that is sensitive to the parameters of implantation temperature and substrate orientation. This model successfully predicts the defect microstructures and relative values of the growth rates found in annealed wafers, as will be seen by comparison to the experimental results.

4.1a Substrate Orientation Effects. When an atom attempts to bond to the surface of a crystal, it will encounter different configurations of bonding sites depending on which crystal face is involved.[33] As a result of the work of Faust,[25,34,35] it has been found that for a silicon atom to successfully attach itself to a silicon crystal it must complete at least two of its four possible bonds. This bonding criterion is more easily satisfied on particular crystal faces as shown in Fig. 12. In this schematic (110) projection of a diamond cubic lattice the unsatisfied bonds on the three major faces, (100), (110), and (111), are shown. Some interatomic distances appear shorter than others only because the bond is inclined to the plane of the drawing. At the (100) face it can be seen that a single atom may attach itself to the surface anywhere, forming two bonds, and thus become a part of the cryatal. At the (110) face a single atom cannot meet this bonding requirement and must first combine with another incoming atom such that the pair may then form two bonds to surface atoms. An alternative sequence of events would be for two

atoms to approach the surface simultaneously and in the proper positions. In any event, growth on the (110) face requires the coordinated motions of two atoms before a stable addition to the crystal has occurred. On the (111) face, bonding is even more difficult. Here, clusters of three atoms are required to satisfy the two bond requirements for each of them. On this basis along, one would expect the growth rate in the [100] direction to be fastest followed by [110] and then [111], which is what is found experimentally.[24,36]

In addition to making qualitative predictions as to the orientation dependence of the regrowth rate, Fig. 12 also gives some insight into the types of defects that are likely to be formed during recrystallization. On the (100) and (110) faces the incoming atoms must join at the proper crystalline positions or they would make first nearest neighbor mistakes. This makes it extremely unlikely that faults will be formed. This is not the case on the (111) face. Here there are two different configurations in which a cluster of three atoms can attach. Both make no first nearest neighbor mistakes. One configuration, labeled "correct" Fig. 12 is the proper one to continue the lattice defect free. The other, labeled "incorrect" makes only second nearest neighbor mistakes and nucleates a twin boundary between the three icoming atoms and the established lattice. The energy of a [111] twin boundary[37] is the lowest of any planar defect for this structure. Therefore the three atom group is almost as stable in this configuration as it is in the correct one. From consideration of this bonding requirement and the atomic structure of various crystal faces

qualitative predictions of relative growth rates for different growth directions, as well as the probability of nucleating twins can be made. However, there are other factors that complicate this picture which I will discuss below.

The surfaces of the crystal in Fig. 12 are all shown to be atomically smooth. In reality some surfaces are atomically rough since they can lower their free energy by assuming a configuration with some atoms in the surface layer missing,[38] as shown schematically in Fig. 13. The rougher surface has a higher entropy but more "dangling" bonds. A rough surface will have a higher density of atomic ledges which will act as sites for easy single atom attachment. Atomic ledges will ease the difficulty of growth on (111) surface and decrease the proability of twin boundary formation.

According to the arguments of Jackson,[39] and the atomic roughness of a surface will be determined by the temperature, entropy of fusion (a material parameter that measures the difference in entropy of an atom in the liquid, or amorphous phase as compared to the crystalline), and the atomic packing density of the surface. Jackson's results indicate that the (100) face of silicon should be atomically rough while the (111) should be smooth at the melting temperature, 1412°C. Hence, these results do not necessarily apply to the present experiments which are conducted in the 500°C to 800°C temperature range. At lower temperature one would expect the surfaces to become atomically smoother, i.e., fewer ledges. Therefore, it is still a safe assumption that the (111) face will be

atomically smooth. But, for the other two major faces, the equilibrium roughness is uncertain.

From the above arguments it can be stated that the growth of a (111) crystal face is reasonably well depicted in the simplistic drawing in Fig. 12, since the (111) surface should be atomically smooth. The (100) face may be rough or smooth, but that is of little consequence since single atoms may easily attach even to a smooth (100) surface. The (110) growth process is an intermediate case with respect to both the atomic roughness and the number of atoms to satisfy the bonding requirements. Hence, it is difficult to state with any certainty, whether ledges are present or even necessary.

The final conclusion is clear: the (100) surface should exhibit rapid and defect free growth for at least one and possibly two reasons. The surface is likely to be atomically rough, thus exposing many favorable bonding sites. Even on a smooth (100) surface, a high density of favorable sites exists and single atoms may easily add on Conversely, growth on a (111) face should be slow and accompanied by twin formation since this surface is atomically smooth and clusters of three atoms which have two possible modes of attachment are required to satisfy the bonding requirement.

Another complication that would invalidate the above discussion is the possibility of surface reconstruction.[40] Reconstruction at a free surface is a change in the crystal structure of the top one or two atomic layers. If this occurs then the ability of an atom to attach to the crystal surface would be drastically affected.

Reconstruction of the surface is known to occur in crystalline silicon in contact with its melt or vapor. The basic driving force for this surface transformation is to minimize dangling bonds which cannot be satisfied by the liquid or vapor. However, a silicon is still covalently bonded and hence there need not be the same kind of discontinuity in bonding across the a/C interface. Because of this, it is much less likely for reconstruction to occur.

4.1b Implantation Temperature Effects. In this section it will be shown how the implantation temperature effect is accounted for in the model for regrowth. Experimentally, it was observed that the roughness of the unannealed a/C interface increased with the temperature of implantation (see Figs. 5,7,8). It is still not clear why implantation temperature has this effect on the interface roughness. However, it may be related to the mechanism of amorphitization and to the degree of mobility of point defects at the implantation temperature.

At high implantation temperatures the initial interface roughness is not governed by the thermodynamic arguments of Jackson,[39] but rather by the radiation damage process itself. At low implantation temperatures, the interface is microscopically smoother (although still not necessarily atomically smooth). During annealing atoms attach to the surface, (100) or (111), in the manner described in the previous section. This results in twins for a (111) wafer, due to stacking mistakes, and dislocation loops (to be discussed in the next section) in (100) after annealing. When the interface is much rougher

there is no well defined growth direction initially since many portions are oriented far away from the nominal plane of the wafer (see Fig. 6C). In the particular case of a (111) wafer with a rough α/C interface, the twins and slow growth rates will no longer be observed initially because many portions of the interface are actually moving in some direction other than [111]. The interface roughness will eventually smooth out, but the maximum α layer thickness for a typical ion implanted wafer is only a few thousand angstroms. If the α/C interface is rough on a scale comparable to this thickness then it may not smooth out before it reaches the surface.

The effect of interface roughness on the regrowth mechanism for (100) and (111) wafers is shown schematically in Fig. 14. for the lowest implantation temperature the interface attains its "equilibrium" state of smoothness almost immediately. This means that the (111) sample forms twins while the (100) first produces a low density of dislocation loops for a very short distance and then produces no defects at all as the interface moves to the top surface. These few dislocation loops are formed during the transition from a microscopically rough to an atomically rough interface and will be explained in greater detail in the next section. At an intermediate value of implantation temperature the transition zone over which the interface becomes smooth is greater. During this period both the (100) and (111) interfaces produce the same type of defects, dislocation loops, and thereafter advance defect free or with twinning, respectively. At the high implantation temperature in

Fig. 14, the transition zone is as large as the total α layer thickness and for this reason both orientations produce the same defects during annealing, dislocation loops.

4.2 The Defect Formation Mechanism During Amorphous Layer Regrowth

In the previous section there was some discussion of the mechanism by which defects could be formed during amorphous layer recrystallization. In this section a more detailed explanation that also includes a discussion of the presence of dislocation loops is presented.

4.2a Dislocation loops and networks. Dislocation loops are commonly found in annealed (100) wafers implanted at all temperatures and (111) wafers implanted at high temperatures. When the loops are smaller than a few hundred Å, they have Frank partial burgers vectors, 1/3 [111]. It is reasonable to conclude that they are a result of condensation of vacancies or interstitial atoms.[41] This is to be expected since the crystalline substrate contains not only a portion of the extra implanted atoms, but many vacancies and interstitials created by radiation damage as well In addition, as the α layer regrows, point defects may be incorporated into the crystal at the α/C interface. During further annealing the existing loops may grow by absorbing free point defects and eventually intersect other loops resulting in dislocation reactions. In this manner a dislocation network can be formed.

If the original α/C interface is very rough, then regions of α material can become trapped within the growing crystalline substrate.

Then as these isolated α zones crystallize, point defects must be generated to compensate for the differences in density of the α and crystalline silicon. This explains why more dislocation loops are found as the implantation temperature, and therefore surface roughness, increases.

It is not the purpose of this study to follow the sequence of events from dislocation loop nucleation to the formation of a stable dislocation network. Other workers[42-44] have addressed this issue and found many interesting aspects. For the purpose of this study, let it suffice to say that dislocation loops are formed in both the crystal substrate and the recrystallized layer after the α/C interface has passed. The loops appear to play no active role in the mechanism by which the α/C interface advances.

4.2b Microtwins. Microtwins are found only in annealed (111) implanted wafers and only if the implantation temperature is less than about 100°C. There are two possible mechanisms for twin formation, the first involving mechanical stresses and the repeated motion of partial dislocations while the second requires atomic growth mistakes. The latter is responsible for the twins formed during regrowth of α layers in silicon. There is no evidence for mehcanical twinning in silicon.

A twin can arise from a stacking mistake in the following way. A diamond cubic crystal can be constructed by adding layers of (111) planes in the proper positions.[45] The stacking sequence is An Bb Cc An Bb Cc. However, if mistakes are made in this sequence planar

defects are formed such as a twins, stacking faults, or microtwins, as shown schematically in Fig. 15. since the (111) interface is atomically smooth repeated nucleation of new atomic layers will be required. The twin boundary energy is 20 ergs/cm^2 (Ref. 37) in silicon so the probability is relatively high that stacking mistakes, such as those in Fig. 15, will occur resulting in twin formation. In this manner twins in the plane of the interface can be explained. However, twins are found inclined to the plane of the interface as well. These twins probably also arise from stacking mistakes. The (111) interface, although atomically smooth, may be faceted on a microscopic scale as shown schematically in Fig. 16. Such a surface will be formed since the interface immediately after implantation is "bumpy", (see Fig. 16a). The fast growing [100] direction, now exposed by these "bumps", will advance rapidly thus leaving behind the slow growing (111) faces. Once this faceted (111) interface is formed, stacking mistakes on inclined planes will be possible. Once an inclined microtwin is nucleated it will grow along with the advancing interface and thus reach a large size as shown in Fig. 16c.

The inclined twin also can benefit further growth as shown schematically in Fig. 17. At the twin boundary only two atoms are required to form a new ledge instead of the usual three on a perfect (111) face. Once a ledge is nucleated, single atoms can attch at this new atomic step. Hence, once the twin is formed, its boundaries act as nucleation sites for further growth.[46] This was first proposed and observed by bennett[47,48] in the growth of dendrites from the melt.

4.3 Comparison of Experimental Results to Model Predictions

The model described in Section 4.1 is not sufficiently refined to predict quantitative values of the regrowth rate of the α layer. However, it does allow one to estimate the relative speeds of interface migration, the types of defects left behind, and the way in which the defects enter into the regrowth process.

4.3a Regrowth Rates. Mayer et al.[49,24] published extensive results of the regrowth rates of ion implanted α silicon layers. They found that the [100] growth direction is the fastest, with the [110] being about three times slower and the [111] about thirty times slower. This is all consistant with the relative difficulty in satisfying the bonding requirement on these surfaces as discussed in Section 4.1a.

4.3b Defect Microstructures. According to the model, the types of defects and the depths at which they should be found, are as follows. For low temperature implantations the (100) sample should contain dislocation loops at the depth of the original α/C interface while the (111) wafer should contain microtwins on all four (111) planes starting at the original α/C interface and extending to the implanted surface. From my own results (Fig. 5) and those of Rechtin[31] et al. the present model is in perfect agreement. For implantations conducted near room temperature, the (100) wafer should contain a wider zone of dislocation loops, starting at the original α/C interface and extending towards to implanted surface. The (111) sample should have this same distribution of loops, but with twins as

well, extending from where the loops end to the surface. Little work has been published on room temperature implantations so the model's predictions may only be compared with the results given in Fig. 7. A higher density of loops is observed in the (100) sample while in (111) loops and then twins nearer the surface are found. The exact depth of these defects was not determined in the present experiments but their approximate positions can be determined by observing wedge shaped TEM specimens where defects at different depths will appear at different distances from the specimen's edge (Figs. 10,11).

At a high implantation temperature, about 100°C, the model predicts identical defect structures for both orientations. This is confirmed experimentally as shown in Figs. 8 and 11 where a dense tangel of dislocations is found in both specimens. In closing, it is apparent that the agreement between theory and experiment, with regard to defect microstructures, is also good.

4.4 Other Models for Amorphous Layer Regrowth

Other models have been proposed to explain the behavior of thin α films as they regrow on crystalline substrates. In a recent paper by Lau,[24] the most prominant of these were reviewed. All but one were clearly inadequate, the work of Csepregi *et al.*[50] being the exception. Their model and the one described here are similar in that both recognized that an incoming atom must form two bonds with the crystal or it is likely to be rejected. However, Csepregi *et al.* did not consider the possiblity that two atoms may link together first and then combine with the surface, as would be required for growth on a

(110) interface. Hence, Csepregi's work does not explain how growth can proceed in the [110] direction. In the [111] growth direction, Csepregi's model predicts a near zero growth rate because nucleation of new atomic steps is exceedingly difficult. He explains the presence of limited growth and subsequent twin formation as a result of ledge nucleation and subsequent stacking mistakes. In this aspect the two models are in agreement. Csepregi et al. suggest that the microtwins once formed will accelerate the growth process since after twinning the new growth direction is [511] which should grow almost as fast as [100]. The twinned region will be in advance of the interface and serve to nucleate growth steps. This prediction is not in agreement with the model presented here.

Even though the [511] twin growth direction is faster, the twin shold soon be bounded by its own slow growing faces, {111}. After this occurs the twin should grow no faster then the rest of the interface as shown in Fig. 18. Lastly, Csepregi's model does not attempt to explain the effect of implantation temperature at all; his model applies only to low temperature implantations.

The effects of implantation temperature and substrate orientation are important aspects of a layer regrowth to be explained but there is one more aspect that is as yet not understood. From Lau's[24] work it is known that a 500-fold change in growth rate is observed depending on which type of ion is implanted. Implanting phosphorus leads to a growth rate 3 or 4 times higher than those found for a silicon implanted silicon specimen. Further development of the model will be necessary to explain this dramatic effect.

5. INTRODUCTION AND RESULTS, TFA SPECIMENS

Thin Foil Annealed (TFA) Specimens TFA specimens are used in this study because they allow the α/C interface to move perpendicularly to the viewing direction. Hence, the role that defects play during interface motion is easily observed. As mentioned before, a single TFA specimen will exhibit growth in several different crystallographic directions. The results from these TFA specimens will be presented according to the wafer orientation from which they were cut since this determines which growth directions will be allowed.

5.1 Results of (001) TFA Specimens

A (001) TFA sample will exhibit growth in two of the major crystallographic directions, [100] and [110], as shown schematically in Fig. 3. Figure 19 shows the defect microstructure of such a specimen that has been completely annealed. Here it is seen that regrowth in the [110] direction is accomplished by a twinning mechanism. This mode of recrystallization is not expected for the [110] direction but rather for [111]. This will be explained in section 6.1a.

In the [100] direction the α/C interface initially advanced by about one micron without forming any defects; this is also shown in Fig. 21. After this distance in the [100] direction, the initially smooth α/C interface broke up into facets and thereafter an extremely high density of microtwins were found. Figure 19d is of a partially annealed (001) TFA sample which shows the extreme sensitivity of the regrowth rate and mechanism on the growth direction. At the exact

[110] direction, the interface has advanced only slightly and the formation of twins is evident. But in adjacent areas where the interface has curved to a different growth direction by just a few degrees, the interface has advanced rapidly and no defects are seen.

From these results it is seen that the TFA samples exhibit a dramatic dependence of the regrowth rate and mechanism on the growth direction, just as has been reported for the conventional specimens[18].

Regrowth rates and the activation energy may be measured in the TEM by taking micrographs of the same area during annealing to monitor the successive positions of the α/C interface. An example of this is shown in Fig. 21 where growth was recorded in the [100] and [110] direction. The numerical data from such experiments is plotted in Fig. 20. Growth in the [100] direction is comparitively rapid, until faceting occurs, afterwhich the growth rate slows by more than an order of magnitude. In the [110] direction, the growth rate is slower than in the initial stages for [100] but remains constant throughout.

In the [110] growth sequence of Fig. 21, the nucleation of a crystallite in the α material is observed. This was found to occur only rarely and in this case can be traced to a foreign particle at the surface. In the [100] sequence of Fig. 21, a larger surface particle is run yet it had no effect on the regrowth process at all. Apparently the surface oxide layer is usually very effective in insulating the amorphous material from foreign particles.

By repeating annealing experiments over a range of temperatures, the activation energy for regrowth may be determined. The practical range of temperatures over which this experiment may be conducted is about 650°C down to 450°C. Outside these limits the annealing times become unreasonably short or tediously long, respectively. In Fig. 20b such data are plotted and an activation energy of 2.9 ± 1 eV is found for both growth directions. Initial stages of growth along [100] are faster than [110] by about a factor of fifteen.

5.2 (111) TFA Samples

In a (111) TFA sample there are two primary growth directions, [110] and [211] types. Long slender microtwins were found in both growth directions, as shown in Fig. 22a. In the [211] case, some of the twins terminated in the later stages of interface migration and further growth took place without the aid of defects. The (111) TFA samples are somewhat complicated by the fact that in one portion of the sample, where the α and crystalline silicon overlap before annealing, microtwins will be formed during annealing since the interface moves in the [111] direction. These twins may then grow out into the unsupported α layer. This may occur even though twin formation might not be required for interface motion in that particular direction. Hence the defect microstructure found in (111) TFA specimens may not be representative of conventional regrowth in the [110] and [211] directions. It is for this reason that numerical data is not reported for regrowth in (111) TFA samples.

5.3 (110) TFA Samples

TFA samples made for (110) wafers are the most interesting of all since they contain all three major crystallographic directions - [001], [110], and [111]. A typical microstructure for regrowth in each of these directions is shown in Fig. 23. In the [111] direction, growth is accomplished by formation of microtwins in agreement with the microstructures in conventional specimens. Growth along [110] produces no defects for a micron or so of growth and then forms a faceted interface after which microtwins are produced. It should be noted that this is identical to the sequence of events for growth in the [100] direction in a (001) TFA specimen. Growth in the [001] direction in a (110) specimen is accompanied by microtwin formation as seen in Fig. 23c. The growth rate data for the [110] and [111] growth directions in the (110) TFA samples are shown in Fig. 24. The results from the (110) samples are disturbing in that the growth rates and microstructures in the [001] and [110] directions are not the same as in the corresponding directions of a (001) TFA sample. Apparently for a TFA specimen, it is only for a particular specimen plane that good agreement is found with the same growth direction in an conventional sample. This unusual effect of the specimen plane will be explained in section 6.1a. Table 1 summarizes the growth rate data obtained from TFA samples.

Table 1. α Layer Regrowth Rates in TFA Specimens (Angstroms/Minute)

Growth Direction / TFA Specimen Plane	Annealing Temperature (C^0) 450	500	550	600	650
[100]/(001)	.84±.05	17.3±.2	243.±5.	2200.±300.	
[110]/(110)		8.7±.5	120.±5.	770. ±100.	
[111]/(110)			16.3±3.	164.±10.	1500.±200.
[110]/(001)	.065±.02	1.1±.2	20.±5.	210±40.	1300.±200.

5.4 General Observation of TFA Specimens

5.4a Contamination Effects. If the TFA specimen is excessively dirty prior to annealing, the regrowth process may be severely affected. Luckily, the effects are usually catastrophic and it is obvious that something is amiss. Typically, one finds a high density of very small, randomly oriented crystallites nucleated in the α layer as shown in Fig. 25.

5.4b. The Effect of Curvature on the Growth Rate. The α/C interface in a TFA specimen will always have some curvature since it follows the edge of the central hole caused by chemical thinning. The α/C interface will be advancing towards its center of curvature and hence growth may be enhanced somewhat. The growth rates in the [100] and [110] direction in an (001) specimen were measured for samples with a wide range of curvature, as shown in Fig. 26. Growth in the [100] direction was not affected by curvature. However, in the [110] direction, below a radius of curvature of abut 20 microns the growth was higher by a factor of two or three. Hence, to obtain reprodicable data only specimens containing fairly large holes, usually on the order of [100] microns in diameter, were used. The fact that only one growth direction is curvature sensitive has important implications which will be discussed in section 6.1b.

5.4c Oriented Crystallites in Advance of the α/C Interface. Crystallites are ocassionally observed slightly in advance of the initial α/C interface in a TFA specimen as shown in Fig. 27. What is unusual about them is that they are perfectly oriented with the crystal substrate. These crystallites are not nucleated but, rather, are a result of a non-uniform chemical attack during specimen preparation. For some reason a few small islands of the crystal substrate are left behind on the α layer. Then, during annealing the isolated crystalline zones will initiate regrowth in advance of the α/C interface as shown schematically in Fig. 27d. The crystallites always form regular shapes such as squares or hexagons which is

explained by them being bounded by the slow growing (111) planes. The growth rates of these crystallites are of some interest since the curvature of the faces is probably zero or slightly negative, that is, the interface is growing away from its center of curvature.

6. DISCUSSION OF THIN FOIL ANNEALED AMORPHOUS LAYER REGROWTH

The TFA experiment is a new technique for observing the mechanism of regrowth of α layers. The unique advantages of this type of experiment have already been mentioned. However, there are several complications, due to the unusual geometry of these specimens, that must be understood before this experiment will be of use.

6.1 Complications in evaluating the TFA Experiment.

6.1a. α/C Interface Rotation and Faceting. The lowest energy plane in silicon is the (111), (1230 ergs/cm^2) followed by (110), (1510 ergs/cm^2) and (100), (2130 ergs/cm^2).[51] If the migrating interface is any plane other than (111) the interface will attempt to rotate towards (111) it during motion to lower its energy even at the expense of some increase in surface area. The ease with which the interface plane can approach (111) will be determined by how near the original interface lies to one of the four (111) planes. For certain growth directions in the TFA experiment, for example [110] in a (001) specimen, the interface must rotate by only about 35° to reach (111) and it can do so by rotating as a single unit. However, in a (110) specimen plane the (110) interface must not only rotate by this angle but break into facets as well, as shown schematically in Fig. 28. When faceting is required for rotation to a (111) interface the transformation is slow to occur but otherwise takes place almost immediately during the first stage of motion. Once the interface assumes the (111) orientation, it displays regrowth characteristics (a very slow growth rate and the production of high density of microtwins)

identical to those found for growth in the [111] direction, even though the apparent direction of interface motion is [110]. It is fortunate that the formation of facets is slow. This allows an interface to move approximately one or two microns while the interface is still perpendicular to the apparent growth direction thus serving as a useful simulation of conventional wafer annealing. The onset of faceting is not related to the decrease in thickness of the α layer as the α/C interface advances. Faceting occurred after one or two microns of growth in specimens with a wide range of wedge angles. It is not presently understood why the α/C interface remains planar for a fixed amount of regrowth, about one microns, and forms facets thereafter. It is likely to be an impurity poisoning effect. Impurities could have diffused in from the free surface, extended completely across the α/C interface, and thus effected the mechanism of regrowth. If this is the case, the observation of an approximately constant regrowth distance before faceting can be understood as a result of a balance of the α layer regrowth rate to the diffusion rate of the impurity.

The concept of interface rotation explains several puzzling results of the TFA experiment. Twinning was found from the start in the [110] growth direction in the (001) samples (from now on this will be designated as [110]/(001)) but in the [110]/(110) case, faceting and subsequent twinning, were found to begin only after a micron of growth. In conventional (110) wafers no twins are found whatsoever. It is suggested that what has happened is that in [110]/(001) the

interface rotated as a single unit and commenced [111] type growth immediately while in [110]/(110) the initial micron of growth was with a true (110) interface until (111) type faceting occurred. Therefore, to observe typical [110] regrowth, the (110) TFA sample must be used and then only for the first micron of growth. To observe typical [100] growth a (010) specimen should be used because here faceting is also the mode of interface rotation and it is delayed as in [110]/(110). Typical regrowth in the [111] direction is found in a (110) TFA specimen.

The assumption that growth in the [110] direction in a (001) TFA specimen is [111] type regrowth since the α/C interface probably rotates to the (111) plane in the initial stages is verified out by the growth rate data in Fig. 24. Here it is seen that identical regrowth rates were found for [110]/(001) and [111]/(110). Hence [111] type regrowth may be observed in both (100) and (110) TFA specimens. The equality of the rates is surprising since one would expect that these two growth rates would differ at least by a geometrical factor since one of the interfaces is moving in a skewed direction.

6.1b <u>The Effect of α/C Interface Curvature on the Regrowth Rate</u>

As mentioned in section 5.4b, curvature of the α/C interface affects the [110]/(001) growth direction but not the [100]/(001). It is now assumed that for growth in the former direction the interface plane is actually (111). Hence the curvature of a (100) interface does not affect its rate of advance while the opposite is true for

(111). This can be explained in the following way. Curvature will produce atomic ledges on a surface as a geometric necessity. However, only if the growth mechanism on a particular interface requires ledge nucleation, will the resulting growth rate be curvature sensitive. The result that only growth in the [111] direction is affected by curvature confirms the hypothesis presented earlier that the (111) α/C interface is atomically smooth and advances by nucleating atomic steps. The fact that the (100) growth rate is unaffected by curvature is not so informative since it only implies that the surface is atomically rough and/or single atom bonding to the crystal surface is easy. Therefore, this experiment does little to distinguish between the two possibilities.

To obtain consistent experimental results the effect of curvature on the growth rate must be avoided. For [100] growth this poses no problem but for [111] one must be carefu to use specimens where the central hole is at least 40 microns in diameter. In practice this is not difficult; in fact, it requires great skill to obtain holes this small. However, local regions where the curvature is greater than the average value must be avoided.

6.1C The Effect of the Doping Profile

As mentioned in section 4.4 the implanted ion species affects the rate at which regrowth occurs. In a conventional wafer there is an approximately Gaussian profile of dopant atoms extending from the implanted surface. As the α/C interface moves toward the surface it encounters at first an increasing and then decreasing dopant density.

Hence the growth rate should not be linear for conventional specimens. The geometry of TFA specimens is such that the α/C interface passes through the entire depth of the α layer, at least initially, and thus will average the effect of the doping profile. As the interface advances towards the edge of the TFA specimen the foil will be thinner and represent a region nearer the implanted surface. This means that the average doping density that the α/C interface experiances will be lower than before. This could result in some nonlinearity of the growth rate if measured over large enough distances. This effect could be avoided by using the multiple voltage implant technique[21,22,52] to obtain a uniform doping profile.

6.2 Comparison of Data from Conventional and TFA Samples

To determine how closely the TFA specimens simulate regrowth of layers in the conventional geometry a comparison is now given of the results of the regrowth rates, activation energy, and defect type from both types of specimens.

6.2a Numerical Data. Mayer's Rutherford backscattering measurements[7,18,20,50] are the most reliable data on α layer regrowth rates and activation energy presently available and are shown in Fig. 20b. He obtains an activation energy for regrowth of 2.4 eV, while I have obtained a value of 2.9 ± 1 eV. Both Mayer's and this study agree that the activation energy is not affected by the growth direction. In a recent study of α layer regrowth, using a thin foil TEM *in situ* annealing experiment, Kooster[59] also obtained a value of 2.9 eV for the activation energy. The significance of these numbers

is not clear at present. They are all well below the activa- tion energy for self diffusion (3.8 eV) and are probably a reflection of a process of atoms hopping across the interface. It is difficult to explain why there should be such a large difference in activation energy for the two experiments. Impurity effects may be different in the thin foil experiment, and these might conceivably effect the activation energy. Another possibility is that the state of stress,[54-57] which will be higher in the conventional wafer since it is constrained in two directions, may supply some of the activation energy required for the α to crystalline transformation. If this is the case, the thermal energy required would be reduced for the conventionally annealed wafer as compared to the TFA specimen. Pinning of the α/C interface at the foil surface could also affect the TFA specimen growth rates.

The relative rates of the [100], [110], and [111] growth directions agree fairly well between the TFA and conventional specimens. Csepregi et al.[50] found [100] to be the fastest direction with [110] and [111] being three and thirty times slower respectively. The present experiments gave the same relative order but the [110] and [111] rates were 2.3 and 15 times slower than [100]. As pointed out in Lau's[24] paper the implanted ion dose and species will affect the regrowth rate. Hence, the numerical data presented here should only be compared with other phosphorus implantations at similar concentrations.

6.2b Defect Microstructures.

If one looks at the defects produced in the [100]/(010), [110]/(110), and [111]/(110) growth systems and compares them to those found in (100), (110), and (111) conventional specimens, respectively implanted at low temperatures, perfect agreement is found. Dislocation loops are found in the [100] and [110] growth directions while twins appear in [111]. The TFA specimens only compare to low temperature implanted wafers because the interface has reoriented itself to be perpendicular to the original α/C interface and in doing so has had sufficient time to smooth out any roughness due to high temperature radiation damage.

In summary the TFA specimens give excellent agreement to the types of defects found in the various growth directions in conventional wafers. The numerical data of growth rate and activation energy are similar for the two experiments but differences definitely do exist which cannot be explained at this time. The possibility exists that the data obtained by the Rutherford backscattering measurements may ontain systematic errors that lead to an incorrect determination of the activation energy. The RBS technique[58] locates the position of the α/C interface by measuring the degree of scattering of alfa particles due to lattice disorder. The α phase is very disordered and causes a dramatic increase in scattering as compared to the perfect crystalline material. However, if the crystal contains a high density of point defects and/or microtwins, as is often the case, the resulting scattering may be sufficient to cause large errors in the determination of the α layer thickness.[(62)] Initial measurements may be

shrouded by the presence of point defects while in the later stages of annealing microtwins will create difficulties. In this way systematic error in the measurement of the α/C interface position during different stages of growth are possible that could give incorrect values of the temperature sensitivity of the regrowth rate.

One of the main advantages of the TFA experiment is that it is a very simple experiment to conduct and may be performed in a short time. In addition to this the TFA technique is the only way in which the role microtwins and dislocating play in the growth process can be directly observed.

7. CONCLUSIONS

7.1 Summary of this Work

A new model for the mechanism of recrystallization of α layers on crystalline substrates has been presented that explains the effects of substrate orientation and implantation temperature. The role of defects in the crystallization process is examined in detail and is consistant with experimental results.

A new technique for observing the regrowth process has been presented. If proper precautions are taken when using the TFA technique excellent agreement of defect structures with conventional specimens is obtained. The TFA experiment shows great promise in further research into other aspects of α layer regrowth.

7.2 Applications to Practical Problems

A good qualitative understanding of α layer regrowth is now at hand. One practical application of this knowledge would be to look at the difficulties in using high dose ion implantation to fabricate an electronic device. When this is done the resulting amorphous layer must be annealed to achieve good electrical activity of the dopant atoms. However, from the result of this work and others, only if the substrate is (100) and the implantation temperature is low, can good results be expected.[16,60] For industrial application it would be beneficial to ease these restrictions. A room temperature implantation would be much more convenient to perform but will leave a rough α/C interface that will produce more defects in the (100) wafer during annealing but fewer in the (111). Hence, if a process to control the

interface roughness could be found improved regrowth from a room temperature implantation might be possible.

There are many other problems related to epitaxial regrowth of a thin layer of one material on another that may benefit from the mechanistic understanding that can be gained from this work. The silicon and sapphire system, where a thin layer of silicon is deposited on a sapphire substrate, is a prime candidate. In this case a high density of microtwins is found which degrades the electrical properties. This is at present an unsolved problem, but similarities exist between this and the α layer recrystallization.

7.3 Suggestion for Further Work

The single most important unanswered question that results from this work is the effect of the implanted ion species and concentration[24] on the regrowth rate and type of defects produced. The TFA experiment is ideally suited to examine this phenomenon. To my knowledge no systematic study has been conducted to determine the relationship of dopant density in the α layer to the regrowth rate. It has been reported that some ion species accelerate regrowth while others slow it down with respect to a silicon ion implantation. The origin of this effect is not understood at present, especially for the case of atomically rough interfaces where regrowth should not take place by a ledge mechanism. A related experiment would be to implant silicon ions into a silicon wafer over a range of doses, all above the amorphitization value. If no effect of the silicon ion dose is found on

the regrowth rate then there must be chemical effects of the ion species. However, if a dependence on the self ion concentration is found then the state of stress or degree of radiation damage must be an important factor in controlling the regrowth rate.

It has been reported that the activation energy for α layer regrowth for some, but not all, implanted ion species is different than for silicon ion implants. However, activation energy data is only available for a limited number of implants at present. There is an enormous amount of useful and interesting work still to be done in explaining the effects of the implanted ion species.

The effect of implantation temperature on α/C interface roughness has no clear explanation at present. Further theoretical study of the radiation damage process in semiconductors may result in a better understanding of this phenomena. In addition, new experiments should be performed to better measure the degree of roughness of the α/C interface. Specifically, by using TEM, cross section specimens[59] the original interface could be seen edge-on such that the roughness can be measured directly. Another novel technique would be to chemically dissolve the α layer away leaving the crystal substrate intact.[24] The exposed interface could then be observed in the SEM or if higher resolution is required, replicas for TEM study could be made since α silicon is slightly soluble in hydrofluoric acid while the cyrstalline form is not,[21,22] hence this is a simple experiment to perform.

Dislocation loops are found in many specimens after the α layer has been annealed. With further annealing they often change burgers vector, grow, change depth in the foil, and intersect to form networks. Although some work[42-44] has already been done on this topic, it is by no means complete. For example, in the present experiments it was found that as the ion dose is increased from 10^{16} to 2×10^{16} phosphorus ions/cm^2, the dislocation loop density found after annealing was drastically decreased as shown in Fig. 29. Further tudies relating network formation to the ion dose, implant voltage and temperature, and ion species are suggested. The nature of the dislocation loops (vacancy or interstitial) has been found by at least one investigator[31] to depend on the implant temperature. In this experiment it was observed that at high implant temperatures and sub-critical doses a completely new type of dislocation loop or precipitate was present that may have been vacancy type and looked very much like those found in boron implanted silicon (Fig. 30). An explanation of this result would be interesting.

With respect to some of the complexities of the TFA experiment there are several topics that could bear further investigation. The reason the α/C interface in the [100]/(010) or [110]/(110) growth system breaks into facets only after one or two microns of growth and not sooner is not clear. A related experiment to this would be to form a very thick α layer (by higher energy implantation) to see if faceting occurs in conventional specimens, as well after the interface has traveled a micron. Another possibility to be investigated is that

impurities might diffuse into the interface during furnace annealing and cause faceting as suggested in section 6.1a. An annealing experiment carried out in ultra high vacuum, if found to eliminate the formation of facets, might resolve this point.

Another interesting aspect of the TFA experiment is the precise dependence of the growth rate on the crystallographic direction. This has been measured for conventional wafers and would serve as a comparison of the two experiments.

One of the differences between the model for regrowth presented in this work and that of Mayer is the manner in which a twin will aid the regrowth process. I feel that the twin boundary is the key while Mayer believes it is the twin's new growth direction, [511], that allows it to advance ahead of the interface. The point could be resolved using high resolution TEM techniques on a TFA specimen.

Another point would be to study the process of nucleation of polycrystals in the α layer. As was stated earlier, this apparently only occurs as a result of contamination, but this has not been proven conclusively. In any event, the new grains are always found to contain defects, probably twins, an obervation which is similar to that made by Kooster.[53] These grains are usually found to nucleate at a position halfway between the original α/C interface and the edge of a TFA specimen. At this location the peak density of dopant atoms is exposed to the free surface of a wedge shaped TEM specimen. It is not known if this is significant or just a coincidence but other studies have shown a correlation of impurity concentration to polycrystalline formation.[61]

A final point of interest concerns the regrowth rates of the α layer in a TFA specimen after the interface becomes faceted. In Fig. 20a, it is seen that this growth is substantially slower than the [110]/(001) growth rate which is actually [111] type growth as pointed out in section 6.1a. According to the model presented in section 4.1a, the [111] growth rate should be the slowest of all. Therefore, it is difficult at this time to explain what has occurred at the α/C interface after faceting that yields such a slow rate of advance. Impurity poisoning is a possibility that should be investigated.

ACKNOWLEDGEMENTS

I would like to acknowledge the influence that my advisor, Jack Washburn, has had on this research. He has given many perceptive suggestions towards solving some of the complex problems that I have encountered. In addition, I was never burdened with pressures to complete this work in a shorter time than was necessary to do a good job.

The help that I have received from my fellow students cannot be overestimated. On many occasions the essential spark for a new idea or experiment was supplied by my colleagues. Had I worked in isolation, there is not doubt this thesis would have taken on an inferior form. However, even more important than technical advice, the friendship that I have experienced has made my stay at Berkeley one that I will always remember fondly. In this respect I would like to thank Carolyn Gosnell, Ken Kubarych, Uli Dahmen, John Sanchez, Tom Shaw and others too numerous to list.

This investigation was performed at the Materials and Molecular Research Division of the Lawrence Berkeley Laboratory. The wo k was supported by the Division of Materials Sciences, Office of Basic Energy Sciences, U. S. Department of Energy under Contract No. W-7405-ENG-48.

REFERENCES

1. J. Mayer et al., Ion Implantation in Semiconductors (Academic, N.Y., 1970).

2. V. Duchynski, Sol. State Tech 20, 53, (1977).

3. M. Barnoski, Sol. State Electr. 16, 441, (1973).

4. H. Muller et al., Applied Physics 4, 115, (1974).

5. J. Gibbons, W. Johnson, S. Mylroie Projected Range Statistics, 2nd Edition (Dowden, Hutchinson, Ross Inc., 1975).

6. M. W. Thompson, Defects and Radiation Damage in Metals (Cambridge Press, 1969).

7. J. Mayer et al., Canadian J. of Phys. 46, 663, (1968).

8. F. Morehead and B. Crowder, Rad. Eff. 6, 27, (1970).

9. J. Dennis and E. Hale, J. App. Phys. 49, 1119, (1977).

10. N. Gerasimenko et al., Radiation Damage and Defects in Semiconductors, Edited by J. Whitehouse (Institute of Physics, London, 1972).

11. F. Morehead and B. Crowder and R. Title, J. App. Phys. 43, 1112, (1972).

12. J. Dennis and E. Hale, App. Phys. Let. 29, 523, (1976).

13. F. Cembali et al., Rad. Eff. 36, 111, (1978).

14. H. Krautle, Rad. Eff. 24, 255, (1975).

15. J. Narayan, R. Young, C. White, J. App. Phys. 49, 3912, (1978).

16. R. Drosd, 9th International Congress on Electron Microscopy, p. 384, (Edited by J. Sturgess 1978).

17. H. Muller et al., App. Phys. Let. 26, 292, (1975).

18. L. Csepregi et al., App. Phys. Lett. 29, 92, (1976).

19. Radiation Effects in Semiconductors, edited by F. Vook (Plenum Press, 1968).

20. C. Cristodulides et al., Rad Eff 36, 73, (1978).

21. E. Kennedy et al., J. App. Phys. 48, 4241, (1977).

22. L. Csepregi et al., J. App. Phys. 48, 4234, (1977).

23. A. Golanski et al., Phys. Stat. Sol. (a) 38, 139, (1976).

24. S. Lau, J. Vac. Sci. Tech 15, 1656, (1978).

25. J. Faust, H. John, J. Phys. Chem. Solids 23, 1119, (1962).

26. S. Ghandi, The Theory and Practice of Microelectronics, p. 135, (Wiley and Sons, 1968).

27. M. Matthews, Rad Eff. 11, 167, (1971).

28. G. Dearnaley et al., Defects in Crystalline Solids, V. 8, Ion Implantation (North Holland 1973).

29. "EECS Laboratory Manual", Berkeley, California.

30. P. Parry, J. Vac. Sci. Tech 13, 622, (1976).

31. M. Tamura, App. Phys. Let. 23, 651, (1973).

32. M. Rechtin et al., Phil. Mag. (A) 37, 605, (1978).

33. Ref. 25, pg. 1119.

34. D. Turnbull, "Thermodynamics in Physical Metallurgy", p. 282, ASM Monogram, (1950).

35. Ref. 50, p. 3909.

36. J. Brice, P. Wiffin, Sol. St. Elec. 7, 183, (1964).

37. J. Friedel, Dislocations (Pergamon Press 1967), p. 158.

38. D. Ulhman, Advances in Nucleation and Crystallization of Glasses, Editors: L. Hench, S. Frieman (The American Ceramic Soc. 1971).

39. K. A. Jackson, Kinetics of Reactions in Ionic Systems (Plenum Press 1969), pg. 229.

40. J. Van Vechten, J. Vac Sci Tech 14, 992, (1972).

41. J. Hirth and J. Lothe, Theory of Dislocations/ (McGraw Hill, 1968), p. 308.

42. S. Mader and A. Michel, Phisica Stdt. Sol. (a) 33, 793, (1976).

43. M. Tamura, Phil. Mag. 35, 663, (1977).

44. N. Gerasimenko et al., Rad. Eff. 37, 167, (1978).

45. P. Wilkes, Solid State Theory in Metallurgy (Cambridge Press, 1973), p. 185.

46. R. Seidensticker and D. Hamilton, J. App. Phys. 34, 3113, (1963).

47. A. Bennett, R. Longini Phys. Rev. 116, 53, (1959).

48. D. Hamilton, R. Seidensticker, J. App. Phys. 31, 1165, (1960).

50. L. Csepregi et al., J. App. Phys. 49, 3906, (1978).

51. A. Jacoodine, J. Electrochem Soc. 110, 542, (1963).

52. R. Allen, Elect. Let. 5, 111, (1969).

53. U. Rooster, Phys. Stat. Sol. (9) 48, 313, (1978).

54. A. Bogh, App. Phys. Lett. 33, 895, (1978).

55. E. Eernisse, App. Phys. Lett. 18, 581, (1971).

56. L. Gerwald, Phil. Mag. (A) 37, 95, (1978).

57. K. Seshan and E. Eernisse, App. Phys. Lett. 33, 21, (1978).

58. Ref. 1, p. 126.

59. D. Sadana, Elect. Let. 13, 632, (1977).

60. K Anand et al., Int. J. Elect. 40, 169, (1976).

61. J. Williams, Rad. Eff. 32, 55, (1977).

62. Foti et al., Phil. Mag. (A), 37, 591, (1978).

FIGURE CAPTIONS

Figure 1. a. Schematic cross section view of a conventional TEM specimen that has been annealed prior to chemical thinning.

b. Schematic cross section view of a TFA specimen that is now ready for annealing.

Figure. 2. A schematic annealing sequence of a TFA specimen where the α/C interface is seen to rotate by 90^0 from its original orientation.

Figure. 3. A schematic view of TFA specimens cut from (100), (111), and (110), wafers. The arrows indicate the different principal growth directions that are found in each specimen.

Figure. 4. A plot of the critical dose required to form an amorphous layer in silicon for three implant species as a function of temperature. Taken from Ref. 11.

Figure 5. Dark field electron micrographs of conventional TEM specimens. Figures a, b, c are of (111), (110) and (100) samples respectively. The (111) sample shows a high density of microtwins while the other two exhibit only dislocation loops. Figure 5b is an unannealed specimen showing the area where the α and crystalline material overlap. The phosphorus ion dose is $10^{16}/cm^2$, implanted at 100kV and then annealed at 800^0C, 1/2 hour.

Figure 6. Figure (a) is a bright field micrograph of a wedged shaped conventional TEM specimen. The inset diffraction patterns show that the upper portion contains both α and crystalline material, while only α silicon is present in the lower half near the edge of the specimen. The bright "speckels" seen in the dark field micrograph, 6b, of the same area can be explained as highly strained crystalline zones in the α/C interface. This is shown schematically in Fig. 6c.

Figure 7. These conventional TEM specimens were all implanted at room temperature. The (111) sample, (a), contains both dislocation loops and microtwins (the latter is verified by the extra spots in the diffraction pattern). The (110), (b) and (100), (c), contain dislocation loops only. Fig. 7d is an unannealed sample where the α and crystalline silicon overlap. All other implantation and annealing conditions are as for Fig. 5.

Figure 8. These conventional TEM specimens were all implanted at 100°C. All three oreintations (111), (110), (100), shown in Figures a, b, c respecitvely, contain dislocation loops and some rods. No twins are found in (111) and no extra spots are seen in the diffraction pattern. The unannealed sample in Figure d is of an area where the α and crystalline silicon overlap. All other implantation and annealing conditions are as for Fig. 5.

Figure 9. These conventional TEM specimens show dislocation networks in a (111),(a), and (100),(b), wafer. The implantation temperature was $100^{o}C$, the dose was $2x10^{16}$ p^{+}/cm^{2} at 100kV, and it was annealed at $900^{o}C$ for 1 hour.

Figure 10. These are wedged shaped conventional TEM specimens where the edge is just off the picture to the right. The left side of these micrographs is a thicker part of the sample. The insets are higher in magnification and show the detailed structure in the thick and thin areas. The sample in (a) was implanted to $77^{o}K$ while (b) was implanted at room temperature. The ion dose in both cases was 10^{16} p^{+}/cm^{2} at 100kV. In Fig. (a) the specimen is somewhat bent such that twins at the right (thin area) have different contrast but are the same as those in the thick region.

Figure 11. These samples are of the same shape as those in fig. 10. The difference is that they are both (100) and the implantation temperature is $77^{o}K$ for (a) and $100^{o}C$ for (b).

Figure 12. This schematic diagram shows how incoming atoms may bond to the surface of an existing crystal. The cross hatched regions show where a new atomic layer has begun. The right hand (111) face has a twin nucleated on it. The viewing direction is 110.

Figure 13. This schematic drawing shows an atomically smooth and atomically rough surface. Note that the atomically smooth surface need not be planar on a macroscopic scale.

Figure 14. This figure is a schematic representation of the effect of implantation temperature of the roughness of the unannealed α/C interface and hence on the recrystallization mechanism. The temperatures indicated as low, intermediate, and high can be taken as approximately equal to 80°K, 300°K, and 100°C.

Figure 15. Symbolic stacking of (111) planes in a FCC lattice showing the different types of planar defects that may result.

Figure 16. Schematic annealing sequence of an α layer on a (111) substrate. The interface is initially somewhat rough but rapidly becomes atomically smooth and forms facets in this process. Thereafter twins, due to stacking mistakes, may be formed on all four sets of (111) planes. Dislocation loops might be formed near the original α/C interface but are omitted for clarity.

Figure 17. This is a schematic (110) projection of a microtwin at a (111) α/C interface. A new atom ledge is seen to nucleate at one of the twin boundaries.

Figure 18. This schematic growth sequence shows how a microtwin will grow in the [511] direction (on a (111) matrix interface) and soon become bounded by its slow growing faces, (111). Thus, boundary nucleation of atomic ledges will be responsible for further rapid growth.

Figure 19. These bright field TEM micrographs are of (001) TFA specimen. Recrystallization has taken place in the exact (111) and (100) directions in Fig(a) and (c) respectively. In Fig.(b) the growth direction is closest to (010), but not exactly, and thus the distance from the original α/C interface to the facets is decreased. This sample was annealed at 800°C for 1/2 hour and is completely recrystallized. Fig. (d) is partially annealed and shows incomplete recrystallization.

Figure 20. Fig. (a) is a plot of the α/C interface position versus time during annealing at 600°C of a (100) TFA specimen for the [100] and [110] growth directions. Figure(b) is a plot of these two growth rates over a range of temperatures. Data from the work of Mayer[22] are also plotted.

Figure 21. Figures(a) and (b) are annealing sequences at 600°C of TFA specimens in the [100] and [110] directions, respectively. The [100] series shows fast growth initially but at 12 minutes, facets are seen to form and thereafter microtwins and a slow growth rate were found. The [110] series shows a slower growth rate than the initial stages of [100], but is constant throughout. Microtwins are continuously formed in the [110] growth direction. A crystallite is nucleated in Fig.(b) at a dirt particle.

Figure 22. Figure (a) and (b) are dark field [112] and bright field [110] growth sequences in a (111) TFA specimen at 575°C. In the portion of the specimen where, prior to annealing, the α and crystalline material overlapped can be seen in the upper portion of each micrograph. Here microtwins are seen since here the α layer recrystallized in the [111] direction. Annealing times, in minutes, are indicated in the upper left corners.

Figure 23. These figures, a, b, c, show typical microstuctures of a partially annealed (110) TFA specimen in the [111[, [110], and [001] directions respecitvely. The original α/C interface is indicated with a dotted line. Twinning occurs immediately in (a) and (c) but a twin free zone is seen in (b) and faceting has just begun.

Figure 24. This is a summary of all growth rate data obtained in this study. The activation energy is constant for all growth directions.

Figure 25. These figures snow the effects of contamination during annealing of a TFA sample. In (a) a single crystal network of "whiskers" has protruded out into the unsupported α layer. The inset diffraction pattern shows both α rings and crystalline spots. Fig(b) shows nucleation of randomly oriented polycrystals.

Figure 26. These two plots show the dependence of the regrowth rate on the curvature of the α/C interface.

Figure 27. Crystalline islands, in advance of the α/C interface, are seen here. Figures(a) and (b) are from a (001) TFA sample while (c) is from (110). A schematic explanation of the origin of these islands is shown in Fig. (d).

Figure 28. This schematic diagram illustrates how the α/C interface may rotate to the (111) planes during migration. This may, or may not, result in faceting.

Figure 29. These are weak beam electron micrographs of conventional TEM specimens annealed at 800°C for 1/2 hour. Both specimens were implanted at 100 keV, the implantation temperature was 77°K, and the substrate is (100). The difference is that the ion dose is $2x10^{16}$ p^{+}/cm^{2} for (a) and only $1x10^{16}$ p^{+}/cm^{2} for (b).

Figure 30. All four figures are conventional specimens implanted at 100°C, at 100 keV. The ion dose is 10^{15} p^{+}/cm^{2} for (a) and (b) while for (c) and (d) it is 10^{16} p^{+}/cm^{2}. Both (a) and (c) are (100) specimens while (b) and (d) are (111). From this it is seen that no substrate orientation difference in defects exists at this implantation temperature. At the higher dose a dislocation network is seen. At the low dose, dislocation loops as well as rod-like defects are found. It is likely at this implantation temperature that an α layer is not formed at the lower dose.

A. Conventional Specimen

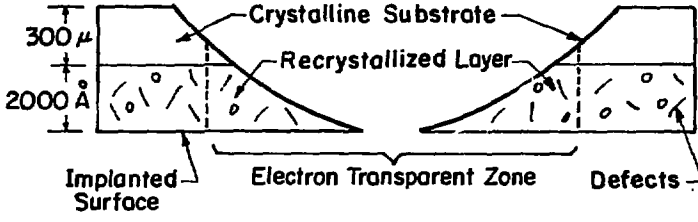

B. TFA Specimen

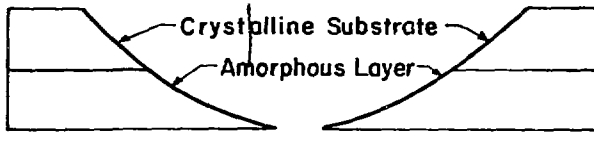

XBL799-7151

Figure 1

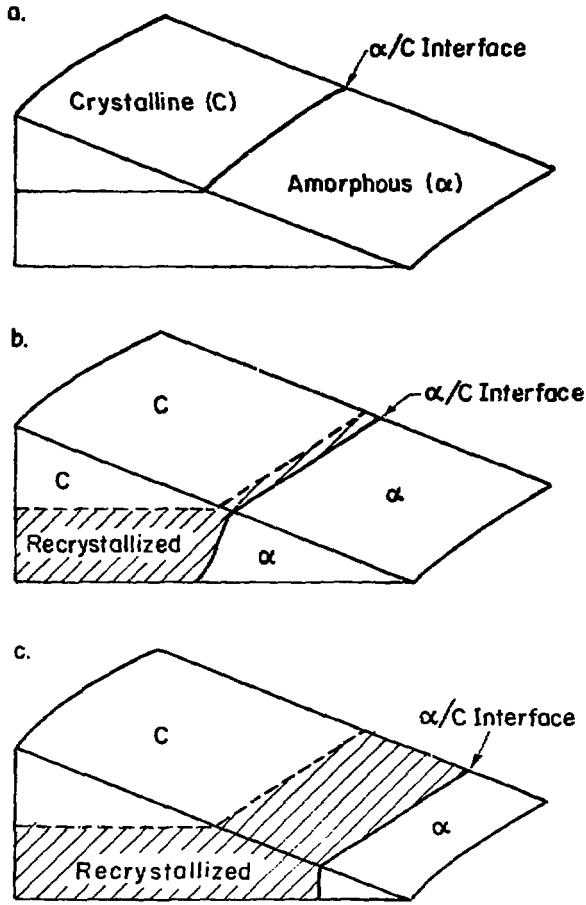

XBL799-7152

Figure 2

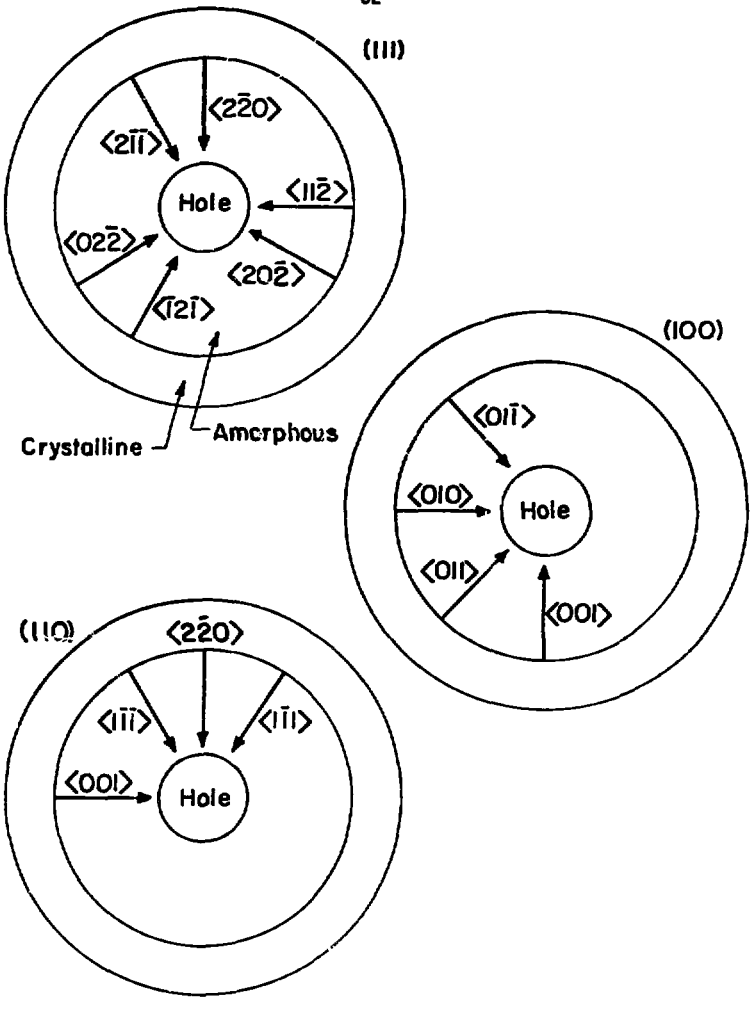

XBL 799-7153

Figure 3

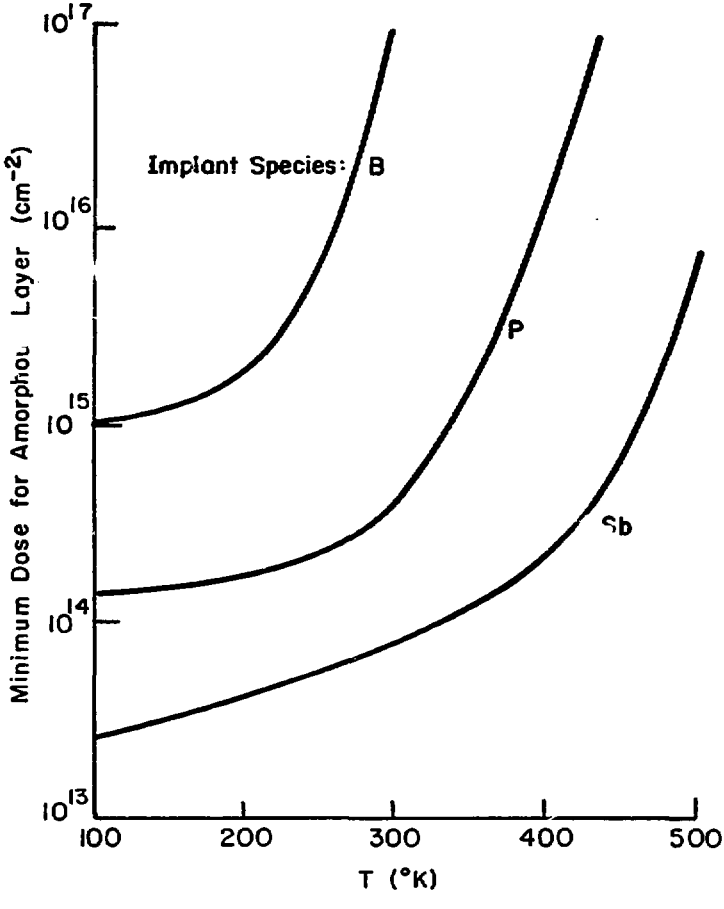

XBL 799-7154

Figure 4

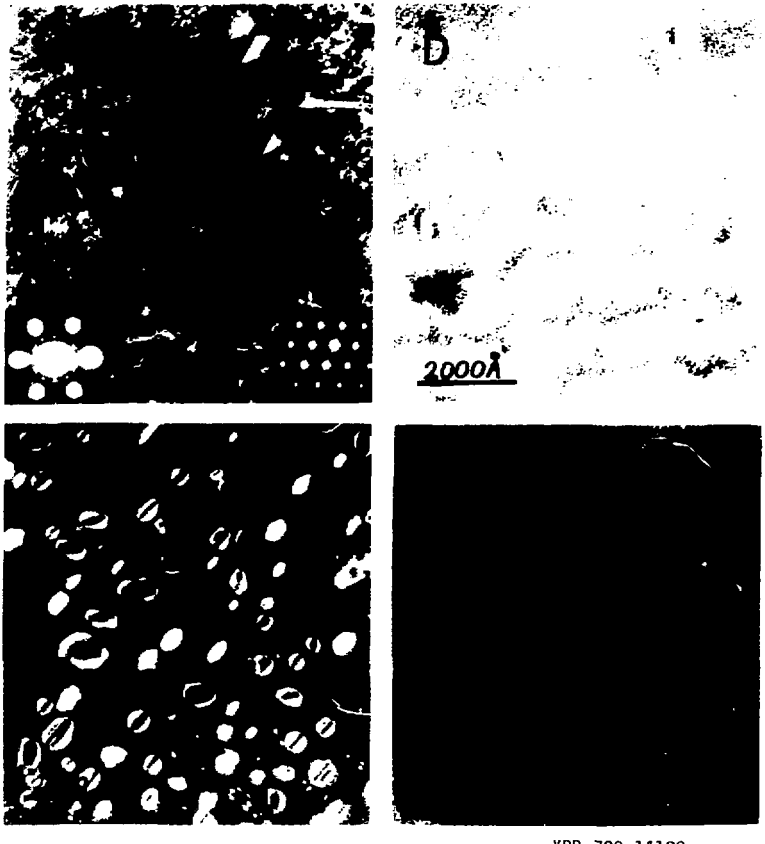

XBB 790-14129

Figure 5

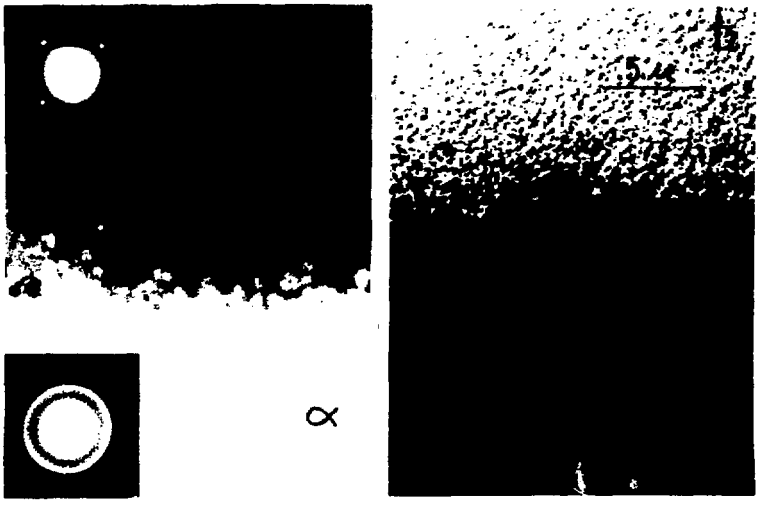

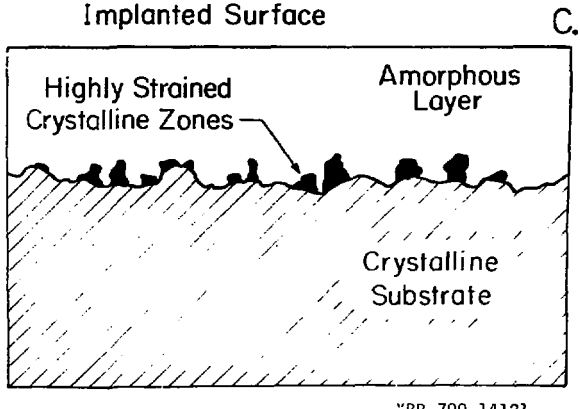

XBB 790-14121

Figure 6

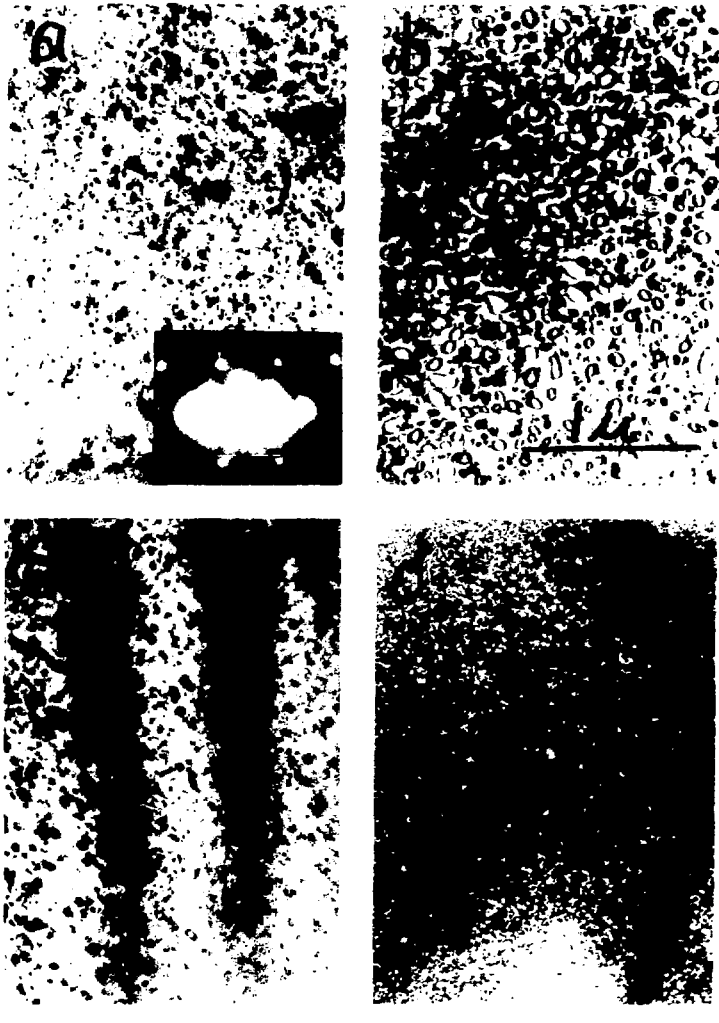

XBB 790-14131A

Figure 7

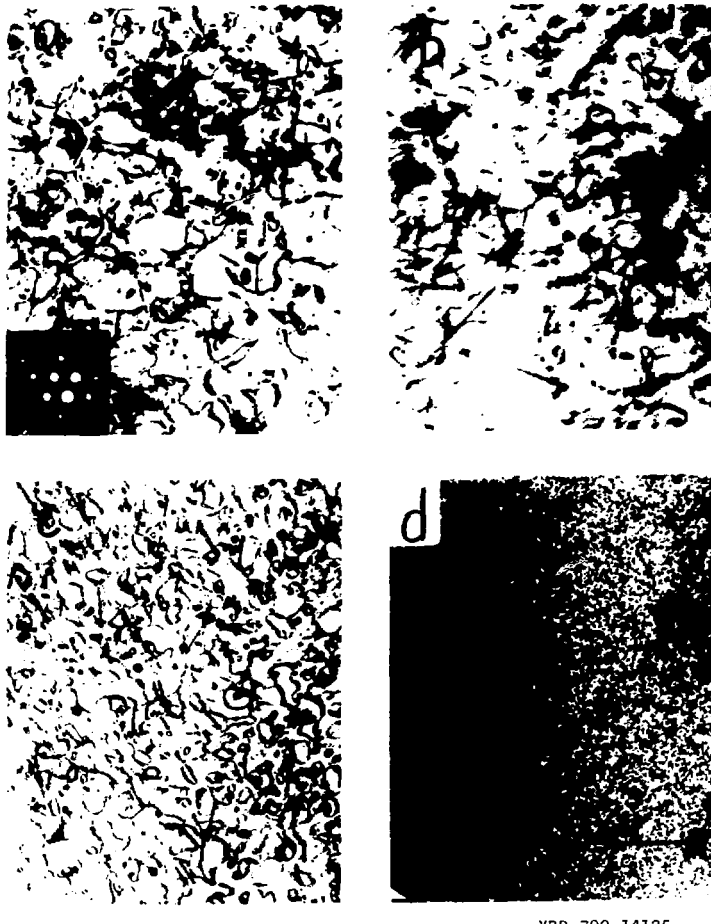

XBB 790-14125

Figure 8

XBB 790-14126

Figure 9

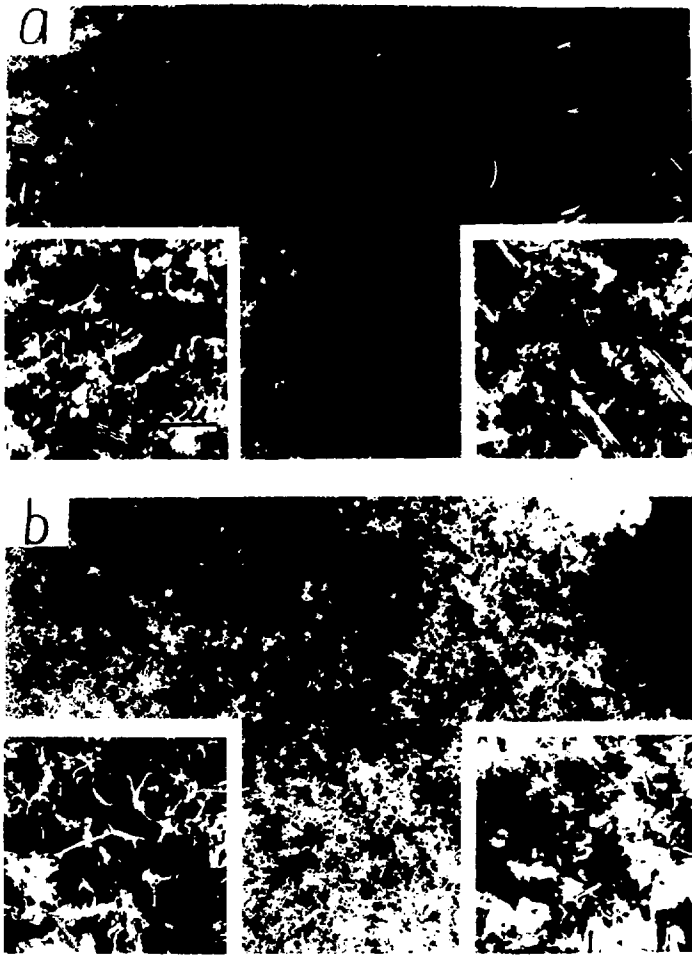

XBB 790-14128

Figure 10

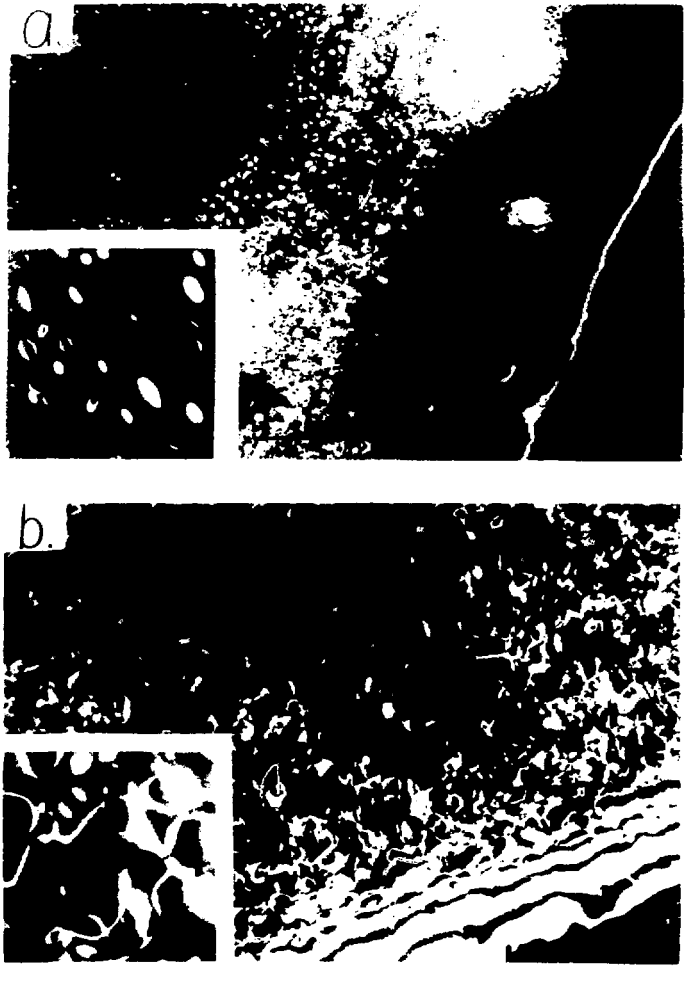

XBB 790-14127

Figure 11

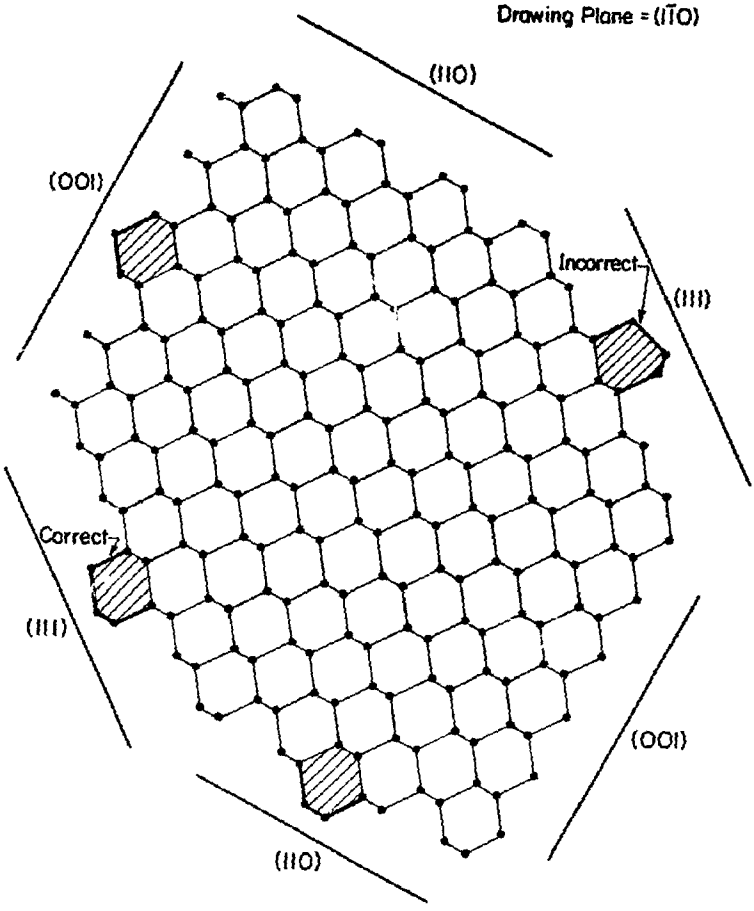

XBL 799-7157

Figure 12

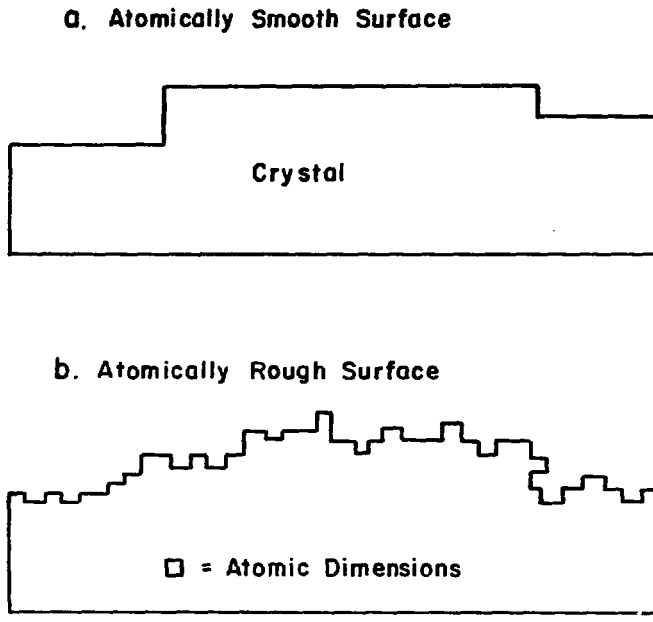

XBL 799-7158

Figure 13

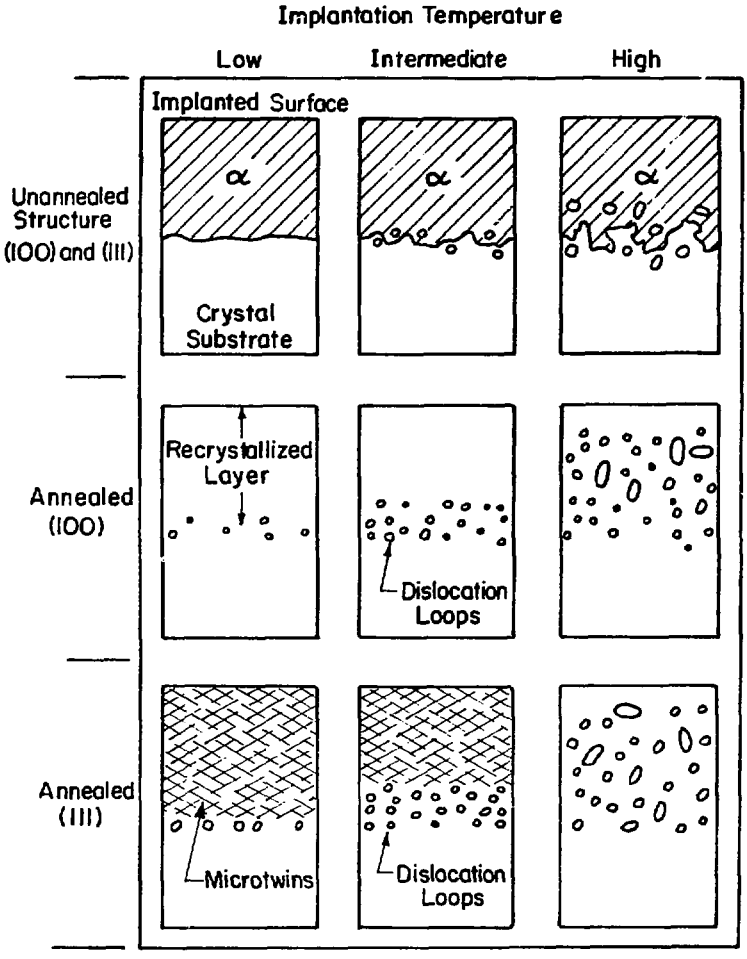

XBL 799-7159

Figure 14

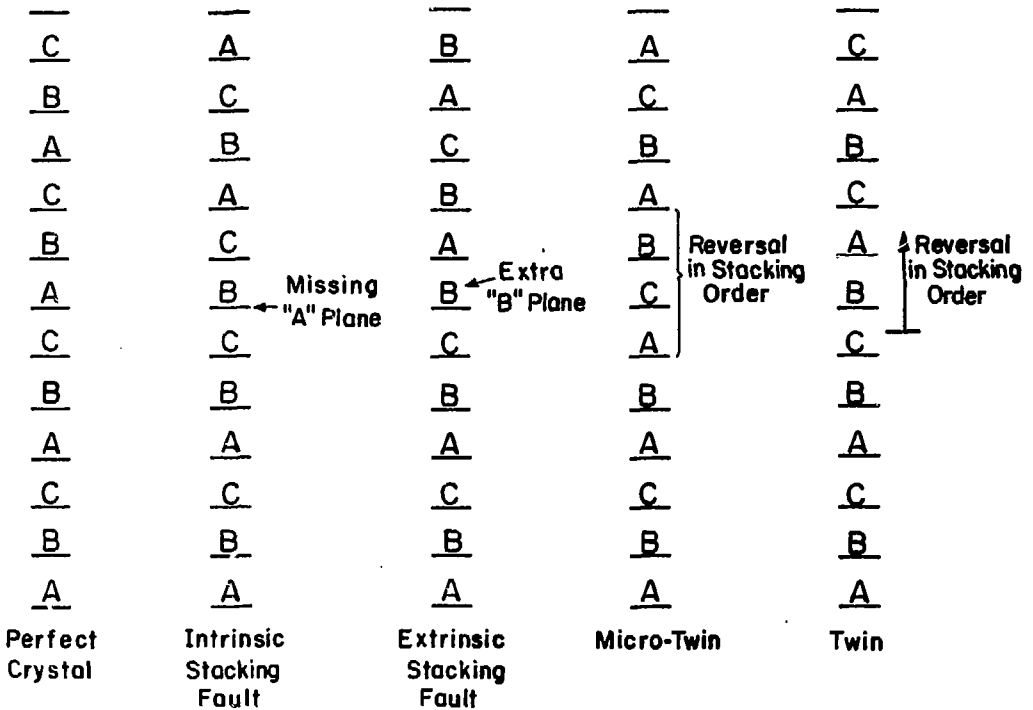

Figure 15

XBL799-7160

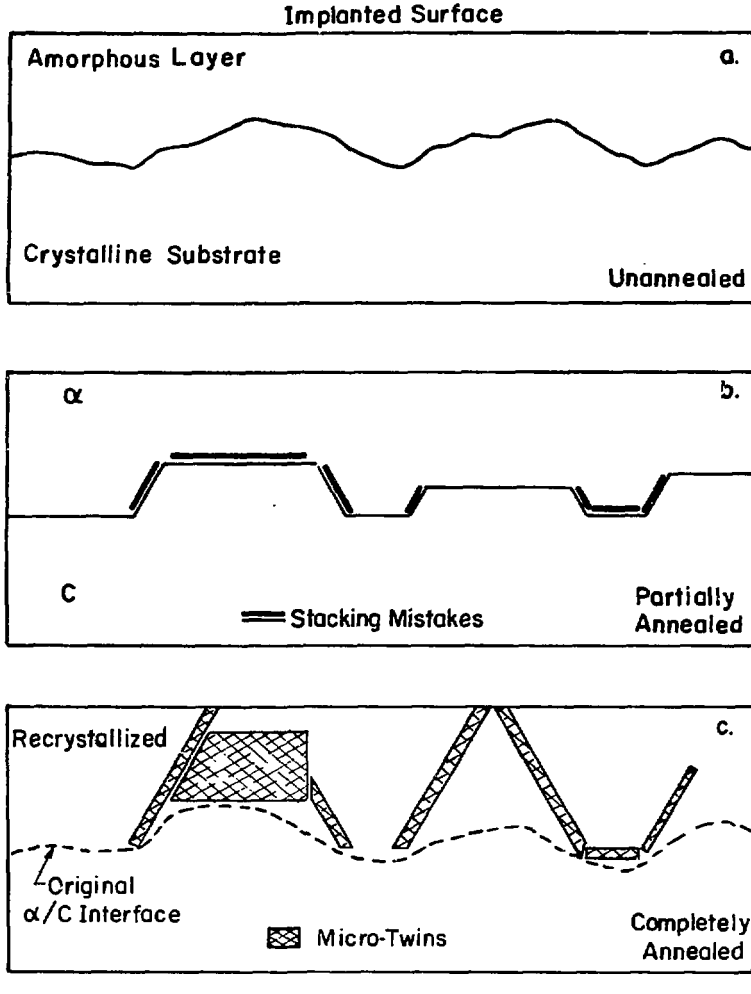

Figure 16

XBL799-7161

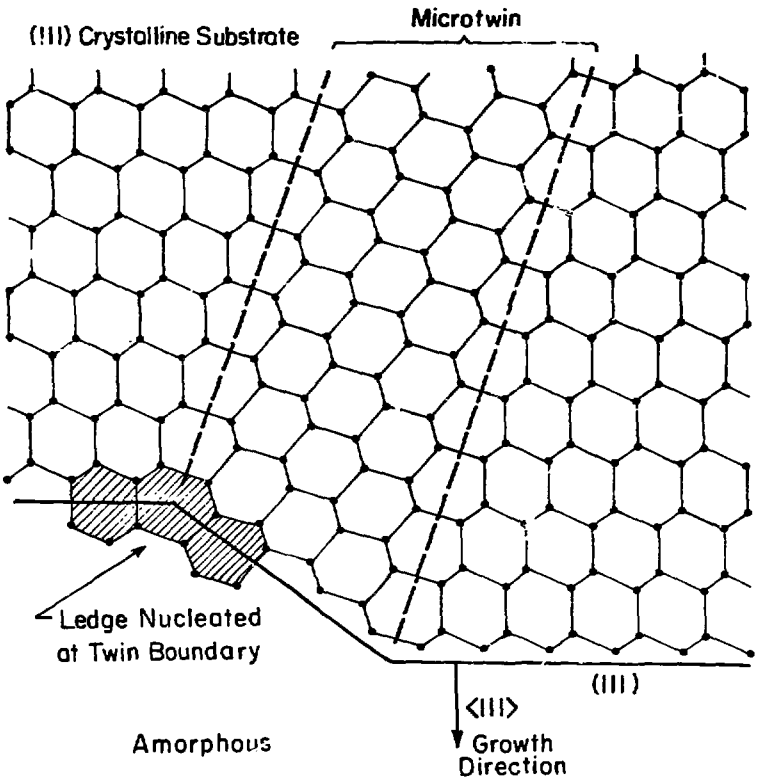

XBL799-7162

Figure 17

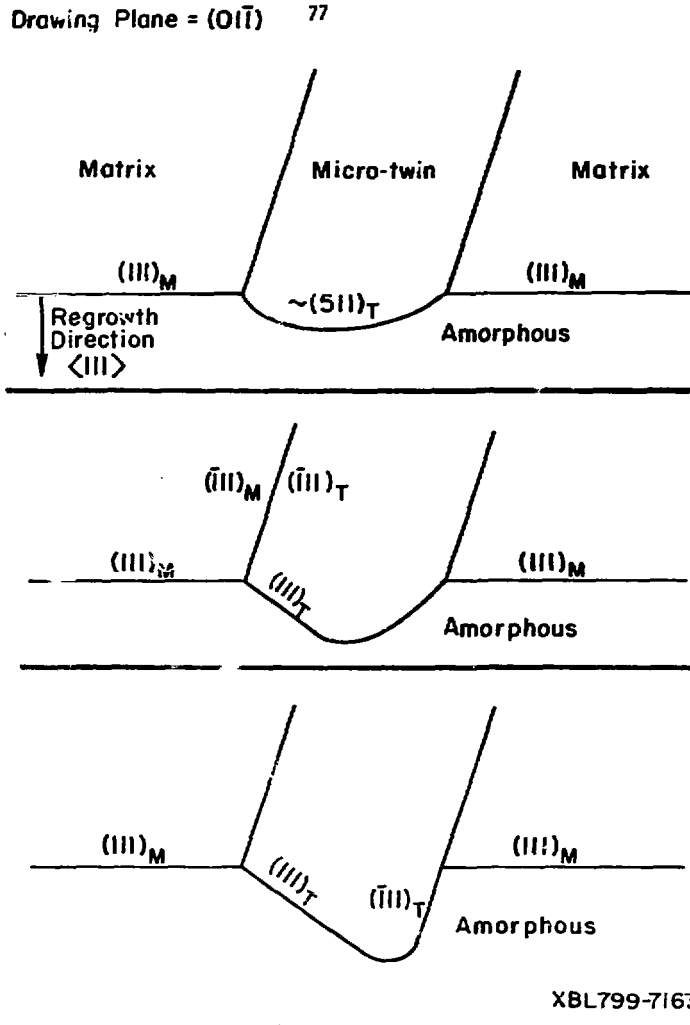
Drawing Plane = (01$\bar{1}$)
Matrix
Micro-twin
Matrix
(111)$_M$
~(511)$_T$
(111)$_M$
Regrowth
Direction
⟨111⟩
Amorphous
($\bar{1}$11)$_M$
($\bar{1}$11)$_T$
(111)$_M$
(111)$_T$
(111)$_M$
Amorphous
(111)$_M$
(111)$_T$
($\bar{1}$11)$_T$
(111)$_M$
Amorphous
XBL799-7163

Figure 18

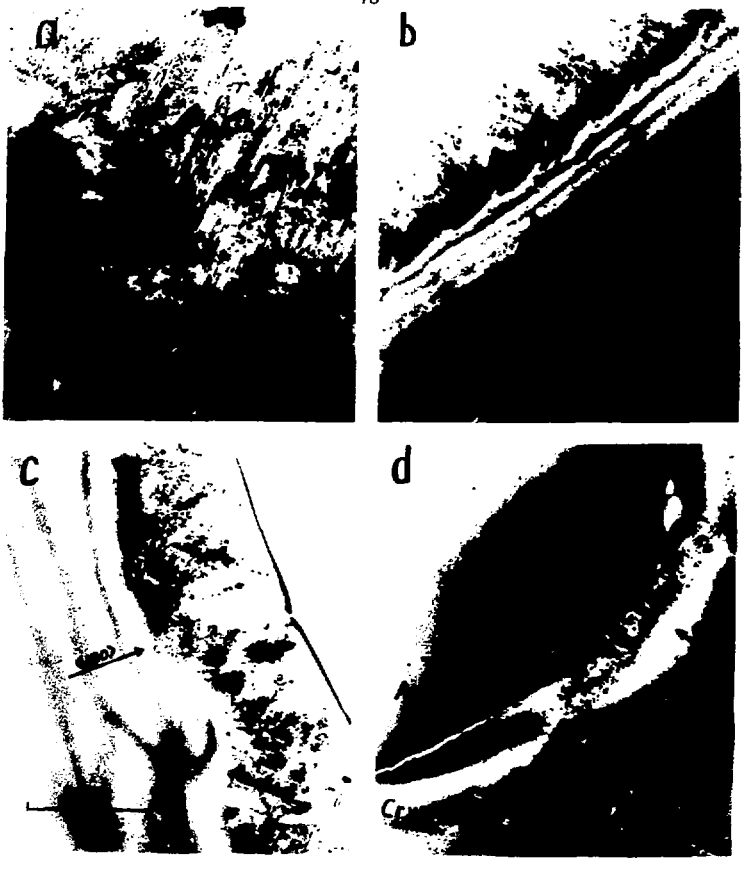

XBB 790-9322

Figure 19

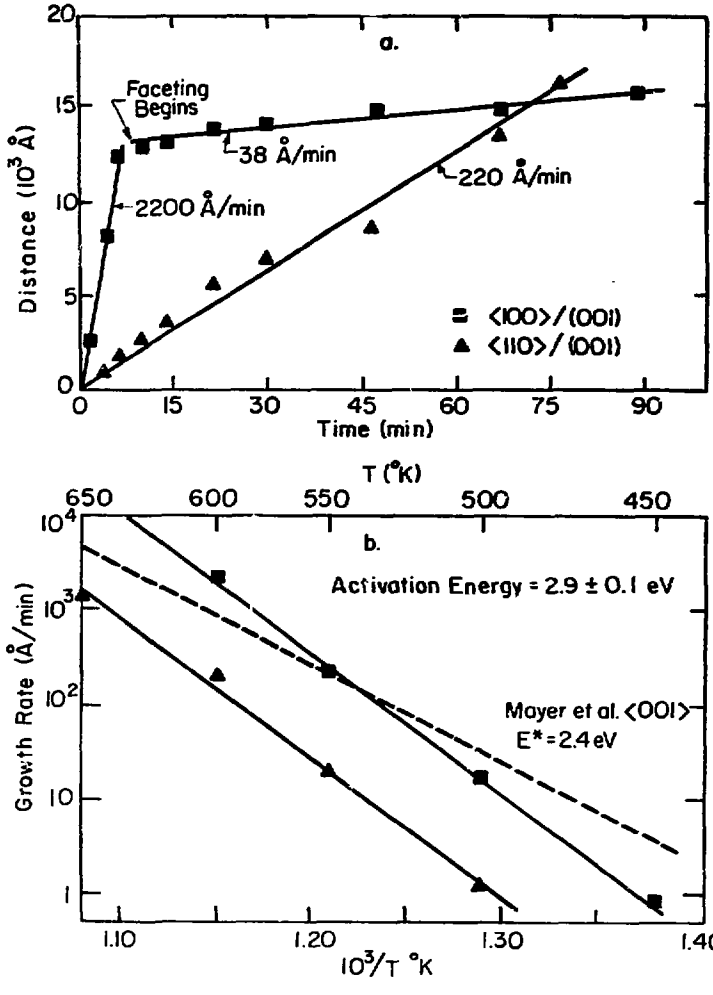

XBL 799-7155

Figure 20

XBB 790-9323

Figure 21

XBB 790-14131B

Figure 22

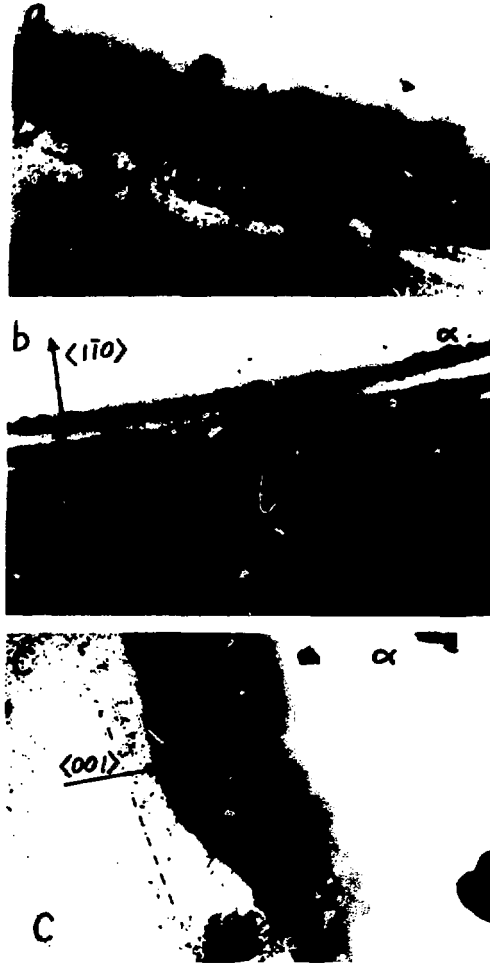

XBB 790-14124

Figure 23

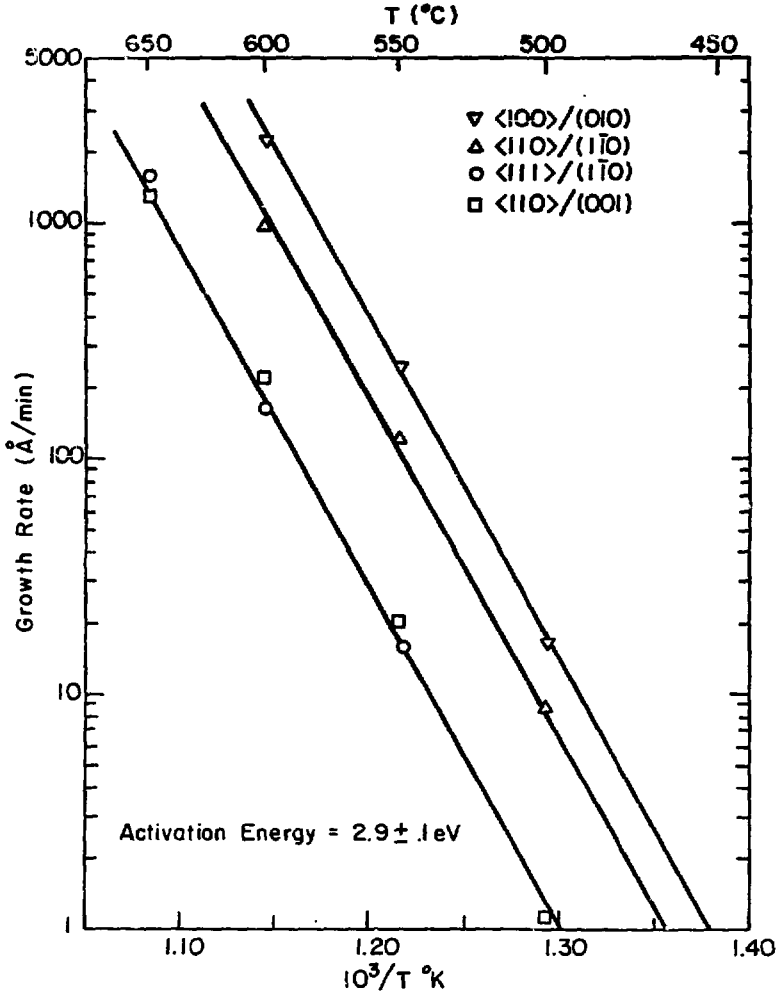

XBL799-7165

Figure 24

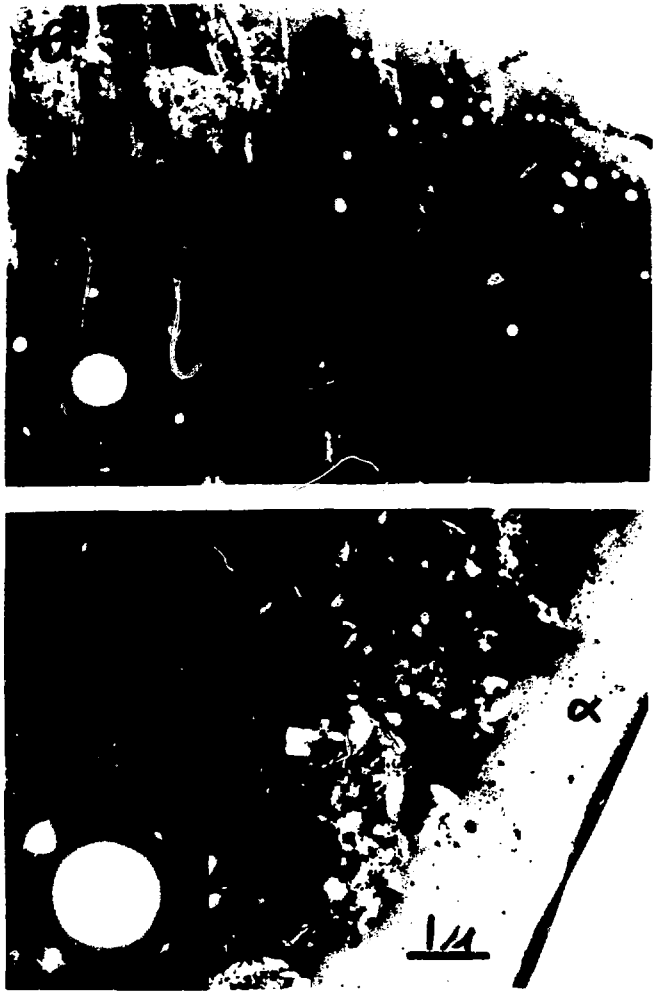

XBB 790-14123

Figure 25

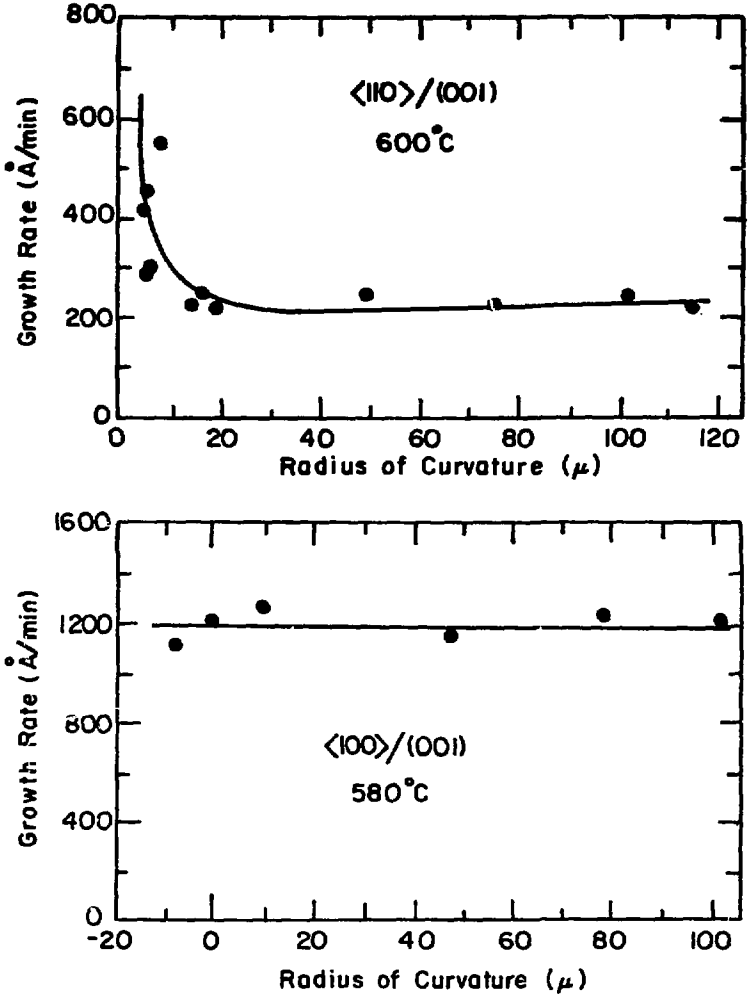

XBL 799-7156

Figure 26

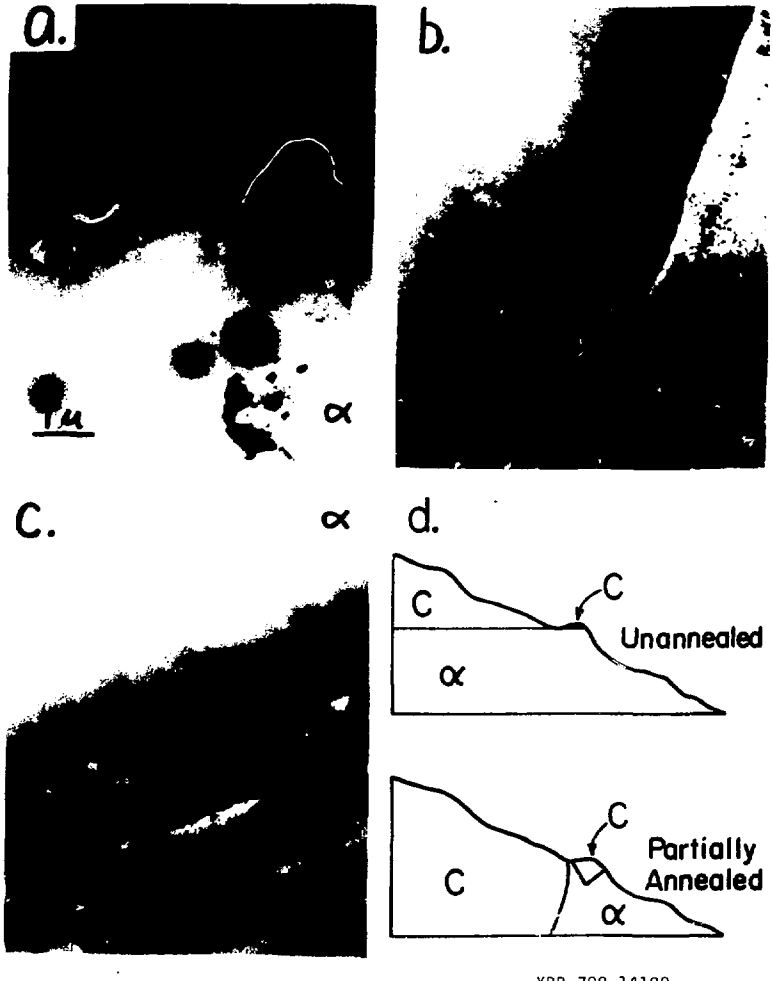

XBB 790-14122

Figure 27

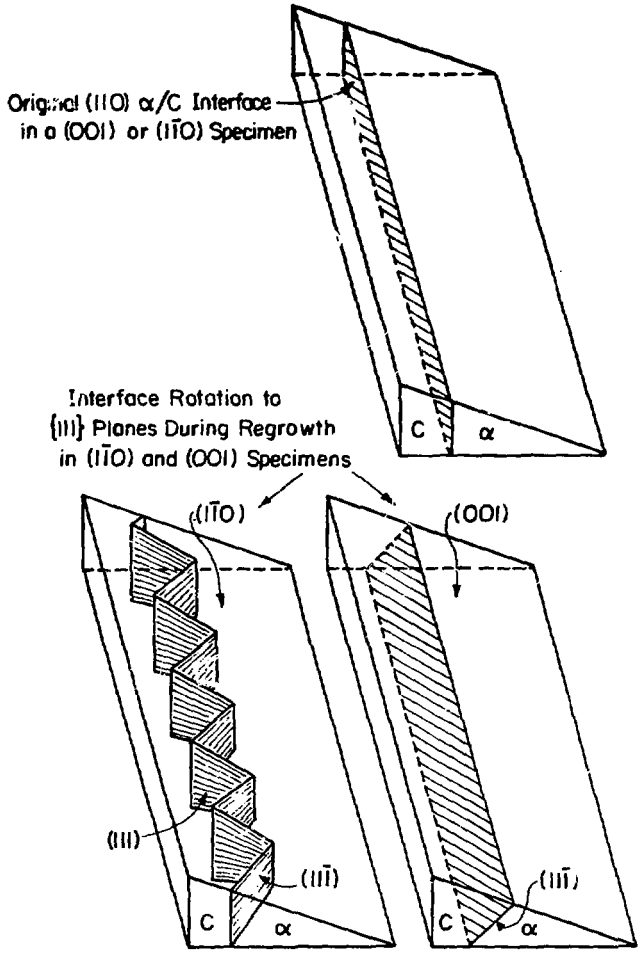

XBL 799-7164

Figure 28

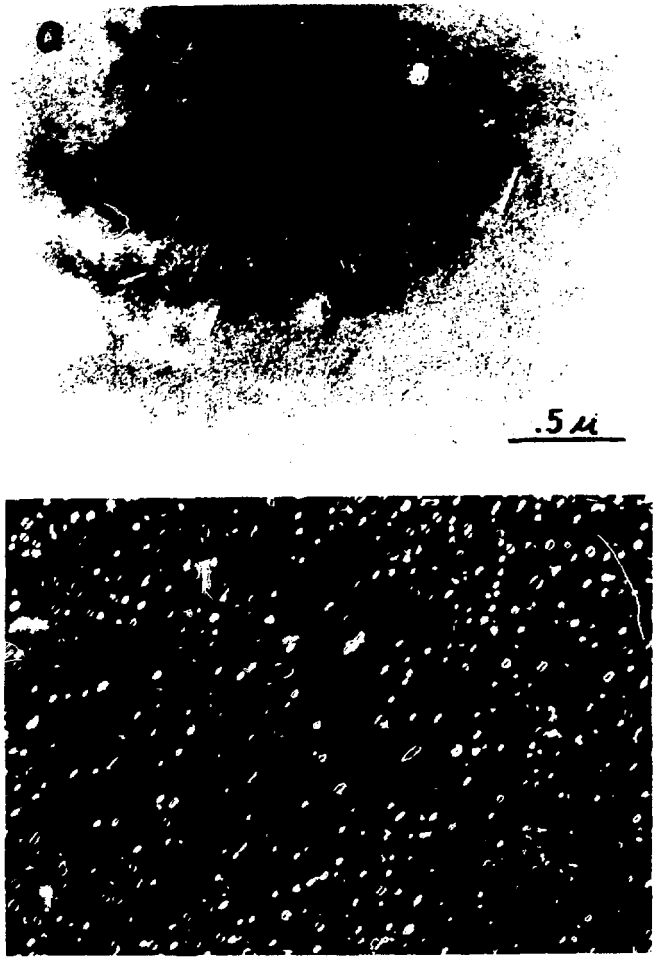

XBB 790-14130

Figure 29

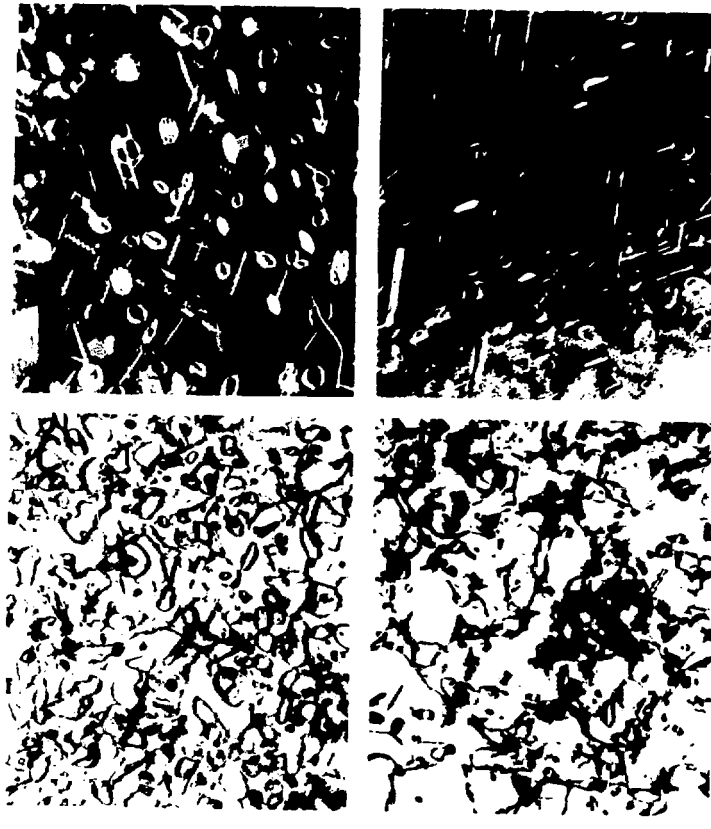

XBB 790-14131

Figure 30